An isospin dependent global nucleon-nucleus optical model at intermediate energies

S.P Weppner,[1,*] R. B. Penney[†],[1,‡] G. W. Diffendale,[1,§] and G. Vittorini[1,¶]

[1]*Natural Sciences, Eckerd College, St. Petersburg FL 33711*

(Dated: November 20, 2008)

A global nucleon-nucleus optical potential for elastic scattering has been produced which matches experimental data to high accuracy and does well in a comparison with other recently formulated global optical potentials. The calculation has been developed for target nuclei from carbon to nickel and is applicable for projectile energies from 30 to 160 MeV. With these ranges it is suitable for describing recent and future experiments performed by exotic beam accelerators. The potential is also fully isospin dependent and has both real and imaginary asymmetry terms to better describe the dynamics of chains of isotopes and mirror nuclei. An analysis of the validity and strength of the imaginary asymmetry term is also included with a comparison to experiment.

PACS numbers: 24.10.-i, 24.10.Ht, 25.40.Cm, 25.40.Dn, 25.40.Kv

I. INTRODUCTION

The fitting of global nucleon-nucleus optical potentials for elastic scattering has a venerable history [1–9]. Recently there has been the development of two modern global optical model potentials (OMP) for nucleon-nucleus elastic scattering which cover an extensive projectile energy and target range: the potentials of Koning and Delaroche [1] and Madland [2]. Specifically the potential of Ref. [1] (KD OMP) has set an impressive benchmark for its extensive projectile energy range (1 keV to 200 MeV) and its accuracy of fit.

The global optical potential of this work (WP OMP) was specifically designed with the next generation of radioactive beam accelerators in mind. First it attempts to fit a lighter and smaller range of targets ($12 \leq A \leq 60$ vs. $24 \leq A \leq 208$ for the KD OMP) and it is also over a more limited projectile energy range (30 MeV $\leq E \leq$ 160 MeV vs. 0.1 MeV $\leq E \leq$ MeV for the KD OMP). This research has also produced one continuous global isospin dependent OMP which covers both proton and neutron scattering. It includes both real and imaginary isovector asymmetry terms to attempt to better describe non-spherical nuclei reactions. Overall the potential of this work is recommended if one is interested in examining trends in the light and medium nuclei, specifically isospin asymmetry dependencies, shell closure, and neutron excess in isotopes. Since the elastic potential formulation is often used as a starting point in developing further inelastic calculations, this global potential will give the user a consistent formulation over a wide range of nuclei.

In section II we will briefly discuss the theory of the global optical potential. A summary of the theoretical fitting procedure and the experimental reactions constraining the fit follows in section III. A generous amount of example calculations are given in section IV which compare the results of this potential with three other contemporary optical potentials. We then analyze, in some detail, the dramatic differences between the strengths of the isovector asymmetry term given by the three global optical potentials in section V. A connection is made to inelastic scattering which is subject to experimental testing. We then end with concluding remarks.

---

[1] Present Address:Department of Physics, Georgia Institute of Technology, Atlanta GA 30332
[†] Present Address:Department of Physics, Florida State University, Tallahassee, FL, 32306
[*]Electronic address: weppnesp@eckerd.edu
[‡]Electronic address: bbp06@garnet.acns.fsu.edu
[§]Electronic address: diffengw@eckerd.edu
[¶]Electronic address: gvittorini3@gatech.edu

II. THEORY

The theoretical and computational aspects of creating a global optical potential has been discussed in detail elsewhere. We mention a few works which we found especially useful. The seminal work of M. A. Melkanoff et. al [10] discusses in great details many of the hurdles that need to be overcome when attempting a computational fitting of nuclear scattering data. F. D. Beccetti and G. W. Greenless [3] created the first comprehensive global optical potential (which is often still used), we especially found poignant their discussion on weighting the various observables. Recently A. J. Koning and J. P. Delaroche have provide the nuclear physics community with an ambitious global optical potential [1] as previously discussed. Their work we have found to be extremely useful for its clear discussion of theoretical issues and its extensive tables on the applicable experimental data that exists.

A. This work

Our complex phenemological optical model potential contains the traditional volume (V), surface (S), and spin-orbit (SO) nuclear terms which are delineated using the standard Woods-Saxon form factors

$$f_{WS}(r,\mathcal{R}_i,\mathcal{A}_i) = \left(1+\exp\left((r-\mathcal{R}_i)/\mathcal{A}_i\right)\right)^{-1}, \tag{1}$$

where $\mathcal{R}_i$ is the radius parameter and $\mathcal{A}_i$ is the diffusive parameter. The i is a placeholder for the V, S, or SO designation. The phenemological optical model potential takes a standard form:

$$\begin{aligned}
&\mathcal{U}(r,E,A,N,Z,MN) = \\
&\Big(-\mathcal{V}_V(E,A,N,Z,MN) - i\mathcal{W}_V(E,A,N,Z,MN)\Big) f_{WS}(r,\mathcal{R}_V,\mathcal{A}_V) \\
&+4\mathcal{A}_S\Big(\mathcal{V}_D(E,A) + i\mathcal{W}_D(E,A,N,Z)\Big)\frac{d}{dr} f_{WS}(r,\mathcal{R}_S,\mathcal{A}_S) \\
&+\frac{2}{r}\Big(\mathcal{V}_{SO}(E,A,N,Z) + i\mathcal{W}_{SO}(E,A,N,Z)\Big)\frac{d}{dr} f_{WS}(r,\mathcal{R}_{SO},\mathcal{A}_{SO})(\mathbf{l}\cdot\sigma) \\
&+f_{coul}(r,\mathcal{R}_C,A,N,Z)
\end{aligned} \tag{2}$$

where the $\mathcal{V}_i$ and $\mathcal{W}_i$ are the real and imaginary potential amplitudes respectively and $f_{coul}(r,\mathcal{R}_C,A,N,Z)$ is the coulomb term which has the following traditional format with a proton projectile:

$$\begin{aligned}
f_{coul}(r,\mathcal{R}_C,A,N,Z) &= \frac{Ze^2}{r}, \quad r \geq \mathcal{R}_C, \\
f_{coul}(r,\mathcal{R}_C,A,N,Z) &= \frac{Ze^2}{2\mathcal{R}_C}\Big(3-\frac{r^2}{{\mathcal{R}_C}^2}\Big), r \leq \mathcal{R}_C.
\end{aligned} \tag{3}$$

For a neutron projectile this term is set to zero. The amplitudes, radii, and diffusive parameters have the following dependent variables:

- **E** – projectile nucleon laboratory energy in MeV
- **A** – Atomic number of the target nucleus
- **N** – Number of neutrons in the target nucleus
- **Z** – Number of protons in the target nucleus
- $\mathcal{P}$ – +1 if projectile is a proton, -1 if a neutron
- **MN** – set to 1 if the target is traditionally singly magic
  – set to 2 if the target is traditionally doubly magic
  – otherwise set to 0.

Explicitly the thirteen Woods-Saxon potential terms are given using twenty-three distinct parameters where one potential term may have up to three parameters. The systematic polynomial formats of these terms are described below. Each of the parameters is purposely numbered to emphasize that each was fitted independently in the process of arriving at the final fit.
The volume amplitudes:

$$\mathcal{V}_V = V_{V_0} + V_{V_1}A + V_{V_2}A^2 + V_{V_3}A^3 + V_{V_5}E + V_{V_6}E^2 + V_{V_7}E^3 \tag{4}$$

$$+ \quad \mathcal{P}(N-Z)\Big(V_{V_{i0}} + V_{V_{i1}}A + V_{V_{i2}}A^2 + V_{V_{i3}}A^3 + V_{V_{i4}}A^4 + V_{V_{i5}}E + V_{V_{i6}}E^2\Big) \tag{5}$$

$$+ \quad MN\Big(V_{V_{m0}} + V_{V_{m1}}A + V_{V_{m2}}A^2 + V_{V_{m3}}A^3 + V_{V_{m5}}E + V_{V_{m6}}E^2\Big), \tag{6}$$

$$\mathcal{W}_V = W_{V_0} + W_{V_1}A + W_{V_2}A^2 + W_{V_3}A^3 + W_{V_5}E + W_{V_6}E^2 + W_{V_7}E^3 \tag{7}$$

$$+ \quad \mathcal{P}(N-Z)\Big(W_{V_{i0}} + W_{V_{i1}}A + W_{V_{i2}}A^2 + W_{V_{i3}}A^3 + W_{V_{i4}}A^4 + W_{V_{i5}}E + W_{V_{i6}}E^2\Big) \tag{8}$$

$$+ \quad MN\Big(W_{V_{m0}} + W_{V_{m1}}A + W_{V_{m2}}A^2 + W_{V_{m3}}A^3 + W_{V_{m5}}E + W_{V_{m6}}E^2\Big). \tag{9}$$

The surface amplitudes:

$$\mathcal{V}_S = V_{S_0} + V_{S_1}A + V_{S_2}A^2 + V_{S_3}A^3 + V_{S_5}E + V_{S_6}E^2 + V_{S_7}E^3, \tag{10}$$

$$\mathcal{W}_S = W_{S_0} + W_{S_1}A + W_{S_2}A^2 + W_{S_3}A^3 + W_{S_5}E + W_{S_6}E^2 + W_{S_7}E^3 \tag{11}$$

$$+ \quad \mathcal{P}(N-Z)\Big(W_{S_{i0}} + W_{S_{i1}}A + W_{S_{i2}}A^2 + W_{S_{i3}}A^3 + W_{S_{i4}}A^4 + W_{S_{i5}}E + W_{S_{i6}}E^2\Big). \tag{12}$$

The spin orbit amplitudes:

$$\mathcal{V}_{SO} = V_{SO_0} + V_{SO_1}A + V_{SO_2}A^2 + V_{SO_3}A^3 + V_{SO_5}E + V_{SO_6}E^2 + V_{SO_7}E^3 \tag{13}$$

$$+ \quad \mathcal{P}(N-Z)\Big(V_{SO_{i0}} + V_{SO_{i1}}A + V_{SO_{i2}}A^2 + V_{SO_{i3}}A^3 + V_{SO_{i4}}A^4 + V_{SO_{i5}}E + V_{SO_{i6}}E^2\Big), \tag{14}$$

$$\mathcal{W}_{SO} = W_{SO_0} + W_{SO_1}A + W_{SO_2}A^2 + W_{SO_3}A^3 + W_{SO_5}E + W_{SO_6}E^2 + W_{SO_7}E^3 \tag{15}$$

$$+ \quad \mathcal{P}(N-Z)\Big(W_{SO_{i0}} + W_{SO_{i1}}A + W_{SO_{i2}}A^2 + W_{SO_{i3}}A^3 + W_{SO_{i4}}A^4 + W_{SO_{i5}}E + W_{SO_{i6}}E^2\Big). \tag{16}$$

The volume radius and diffusive terms:

$$\mathcal{R}_V = R_{V_0} + R_{V_1}A + R_{V_2}A^2 + R_{V_3}A^3 + R_{V_5}E + R_{V_6}E^2 + R_{V_7}E^3, \tag{17}$$

$$\mathcal{A}_V = A_{V_0} + A_{V_1}A + A_{V_2}A^2 + A_{V_3}A^3 + A_{V_5}E + A_{V_6}E^2 + A_{V_7}E^3 \tag{18}$$

$$+ \quad \mathcal{P}(N-Z)\Big(A_{V_{i0}} + A_{V_{i1}}A + A_{V_{i2}}A^2 + A_{V_{i3}}A^3 + A_{V_{i5}}E + A_{V_{i6}}E^2 + A_{V_{i7}}E^3\Big). \tag{19}$$

The surface radius and diffusive terms:

$$\mathcal{R}_S = R_{S_0} + R_{S_1}A + R_{S_2}A^2 + R_{S_3}A^3 + R_{S_5}E + R_{S_6}E^2 + R_{S_7}E^3, \tag{20}$$

$$\mathcal{A}_S = A_{S_0} + A_{S_1}A + A_{S_2}A^2 + A_{S_3}A^3 + A_{S_5}E + A_{S_6}E^2 + A_{S_7}E^3, \tag{21}$$

the spin-orbit radius and diffusive terms:

$$\mathcal{R}_{SO} = R_{SO_0} + R_{SO_1}A + R_{SO_2}A^2 + R_{SO_3}A^3 + R_{SO_5}E + R_{SO_6}E^2 + R_{SO_7}E^3 \tag{22}$$

$$+ \quad \mathcal{P}(N-Z)\Big(R_{SO_{i0}} + R_{SO_{i1}}A + R_{SO_{i2}}A^2 + R_{SO_{i3}}A^3 + R_{SO_{i5}}E + R_{SO_{i6}}E^2 + R_{SO_{i7}}E^3\Big), \tag{23}$$

$$\mathcal{A}_{SO} = A_{SO_0} + A_{SO_1}A + A_{SO_2}A^2 + A_{SO_3}A^3 + A_{SO_5}E + A_{SO_6}E^2 + A_{SO_7}E^3, \tag{24}$$

and finally the the coulomb radius term:

$$\mathcal{R}_C = R_{C_0} + R_{C_1}A + R_{C_2}A^2 + R_{C_3}A^3 + R_{C_5}E + R_{C_6}E^2 + R_{C_7}E^3 \tag{25}$$

$$+ \quad \mathcal{P}(N-Z)\Big(\frac{2Z}{A}\Big)^{\frac{1}{3}}\Big(R_{C_{i0}} + R_{C_{i1}}A + R_{C_{i2}}A^2 + R_{C_{i3}}A^3 + R_{C_{i4}}A^4 + R_{C_{i5}}E + R_{C_{i6}}E^2 + R_{C_{i7}}E^3\Big). \tag{26}$$

Parameters which are rarely used in other global optical potentials are the real surface amplitude (Eq. 10), imaginary asymmetry $(N-Z)$ (Eqs. 8,12,16), geometric asymmetry (Eqs. 19,23,26), and the magic number dependent terms (Eqs. 6,9). The asymmetric parameters and their ramifications are discussed in section V. The magic number terms add some depth to the real and imaginary central potential to better describe the stronger bonding that occurs in these nuclei. We chose to use a non-traditional coulomb asymmetric parameter instead of the coulomb correction potential term which is now common in other global optical potentials. The twenty three parameters which describe the thirteen potential terms are listed in table I.

This potential was put into a standard optical potential calculator which solves the Schrødinger equation for spin $\frac{1}{2}$-spin 0 using a distorted born wave approximation in a coulomb basis (DWBA). We used TALYS [12, 13] which uses ECIS [14] to calculate the solution once the final product was developed. We have produced a Java applet [11] which contains our own optical potential calculator as well as some useful input files for use in TALYS and ECIS which will let one produce results using our global optical potential quickly.

The gestation of the parameters will be described in section III but we will first give an overview of the theoretical structure of this and the other recent global optical potentials.

Term	0	1 (A)	2 (A^2)	3 (A^3)	4 (A^4)	5 (E)	6 (E^2)	7 (E^3)
V	+5.703E1	+4.099E-1	-8.656E-3	+5.793E-5	—	-5.881E-1	+1.822E-3	—
V_i	-7.810E0	+1.054E0	-4.616E-2	+8.384E-4	-5.416E-6	-6.729E-3	+3.684E-5	—
V_m	-3.723E-1	+6.563E-3	-5.308E-4	+7.987E-6	—	+2.515E-3	-5.607E-6	—
W	-1.897E0	-1.843E-1	+5.034E-3	-3.814E-5	—	+2.367E-1	-1.423E-3	2.556E-6
W_i	+8.216E0	-8.359E-1	+3.221E-2	-5.426E-4	+3.320E-6	+8.446E-3	-2.644E-5	—
W_m	-3.781E0	+1.818E-1	-4.772E-3	+3.374E-5	—	+4.157E-2	-2.149E-4	—
V_S	-4.612E-1	-1.178E-2	+9.658E-4	-1.270E-5	—	+7.906E-3	-4.230E-5	—
W_S	+6.189E0	+1.740E-1	-4.790E-3	+3.670E-5	—	-6.423E-2	-3.753E-4	+3.096E-6
W_{S_i}	+3.471E0	-4.265E-1	+1.670E-2	-2.828E-4	+1.744E-6	+1.449E-2	-8.093E-5	—
V_{SO}	+1.562E1	-1.202E-1	+1.765E-3	—	—	-1.923E-1	+1.168E-3	+2.400E-6
V_{SO_i}	-3.666E0	+7.228E-1	-3.524E-2	+6.493E-4	-4.151E-6	+2.472E-3	-3.317E-6	—
W_{SO}	+3.929E-1	+1.660E-1	-5.369E-3	+4.646E-5	—	-3.702E-2	+9.223E-5	—
W_{SO_i}	+5.399E0	-4.639E-1	+1.718E-2	-2.809E-4	+1.696E-6	-1.720E-2	+1.234E-4	—
R_V	+1.491E0	-1.971E-2	+5.447E-4	-4.561E-6	—	-6.255E-3	+9.064E-5	-3.187E-7
A_V	+1.933E-1	+3.484E-2	-9.172E-4	+6.999E-6	—	+5.762E-3	-6.097E-5	+1.929E-7
A_{V_i}	+2.207E-3	+5.253E-3	-1.970E-4	+2.043E-6	—	-5.014E-4	+1.898E-6	—
R_S	+8.599E-1	-5.657E-3	+8.884E-5	+7.253E-7	—	+1.024E-2	-4.166E-5	—
A_S	+9.477E-1	+5.097E-3	+1.201E-4	-2.824E-6	—	-1.255E-2	+4.597E-5	—
R_{SO}	+8.293E-1	+3.098E-2	-7.747E-4	+6.035E-6	—	-3.894E-3	+1.799E-5	—
R_{SO_i}	-1.132E-1	-5.916E-4	+3.596E-6	—	—	+4.458E-3	-4.652E-5	+1.521E-7
A_{SO}	+9.239E-1	+3.091E-2	-7.702E-4	+5.982E-6	—	-1.874E-2	+1.576E-4	-4.161E-7
R_C	+3.604E0	-2.103E-1	+7.753E-3	-8.155E-5	—	+1.074E-1	-6.348E-4	—
R_{C_i}	+3.404E-1	-1.038E-1	+1.294E-3	—	—	+4.501E-2	-3.729E-4	+9.467E-7

TABLE I: Model parameters for the subject of this work, the WP global optical potential Each term is a 5 to 7 term separable polynomial in A are E which are given in Eqs. 4-26. Tools have been developed to facilitate the use of this potential [11].

B. Theoretical comparison with other global optical potentials

The general design of all three potentials under study (KD [1], MD [2], WP) is the same. They use the same base Woods-Saxon functional form which include volume and spin-orbit terms. Additionally the KD and WP optical potentials include surface terms. The KD and MD potentials also include an additional coulomb correction term. Both the WP and MD produce one potential that is utilized for both proton and neutron scattering while the KD potential has separate potentials for the isospin dependence of the projectile.

The KP optical potential imaginary parameters are determined by a dispersive relationship form which is dependant on the difference between the projectile laboratory energy and the Fermi energy of the target as well as constants used in the creation of the real component of the potential. Of the three optical potentials discussed it has the deepest theoretical underpinnings and given these dispersive constraints and high accuracy it has successfully pushed the theoretical development of the global optical potential to a new level.

The goal of the MD potential [2] is to describe the elastic scattering data sets using as few parameters as possible. It uses constants, linear, and the occasional quadratic forms to describe all of its Woods-Saxon parameters. It is quite impressive that a high quality isospin dependent potential was produced with so few parameters.

In contrast this work (WP) uses quadratic, cubic, and quartic polynomials that have no direct relationship to dispersion theory. It has the highest amount of adjustable parameters of the three potentials. What it achieves is ease of use, good asymmetry and mirror nuclei analysis, and complete separability between the nucleon (A) and energy (E) parameters. This WP potential also includes imaginary vector isospin asymmetry ($N-Z$) terms which neither of the other potentials have. In section V we will compare the isovector differences of these three optical potentials in some detail.

III. PROCEDURE

This research tried ambitiously to minimize a χ^2 on over three hundred different nucleon-nucleus experiments by adjusting the polynomial fit to the twenty three parameters given in Table I. To attempt to decouple the terms from each other, the twenty-three values were varied using a systematic method detailed below. A listing and discussion of the experimental dataset follows.

A. Calculation Techniques

The fitting elastic nucleon-nucleus code was developed by two of the authors (S. Weppner and R. Penney). We used a Numerov routine found in Ref. [10] to solve the non-relativistic position space Schrødinger equation in a coulomb basis with a relativistic correction found in Ref. [5]. The routine which produced the coulomb wave functions was found in Ref. [15]. A Powell routine, adopted from Numerical Recipes [16], was used to minimize a weighted χ^2 (proportional to the square of the difference between the theoretical fit and the experimental data).

The code was developed to run on a multi-processor parallel system. Each processor was assigned at least one nucleon-nucleus experimental data set at a given energy and nucleon number (A). This could be as simple as one experiment or many experiments including the observables of total neutron cross-section, total reaction cross section, differential cross section, and polarization. Each set contained, if available, both proton and neutron observables and varying target proton numbers that all shared a common target nucleon number and projectile energy. For example $A = 40$, $E = 40MeV$ data exists to have a proton striking ^{40}Ca and producing a total reaction cross section observable, a differential cross section, and polarization. These were fit along with a neutron striking ^{40}Ca and producing a differential cross section, a total reaction cross section and a total cross section and also including a proton at 40 MeV striking ^{40}Ar and producing a reaction and differential cross section. All eight of these experiments made up a complete working data set in which the parameters were varied and the minimization routine for the weighted χ^2 was executed. By analyzing many different data sets at the same energy and nucleon number we intended to reduce systematic error and ultimately derive a better global fit among chains of target nuclei.

Each fit cycle contained a three step process. First all parameters were adjusted except three (the two magic number terms and the asymmetry coulomb term (Eqs. 6,9,26). Since the other twenty were being adjusted simultaneously it was important to analyze only a subset of the entire dataset to avoid ambiguities within the parameter space. The datasets used contained either only $N = Z$ targets or sets in which a variety of different Z targets existed for a fixed nucleon number and fixed projectile energy or sets in which neutron and proton projectile observables existed for that fixed A and fixed projectile energy E. These sets therefore either had no $N - Z$ dependence or it was clearly delineated by including a variety of elements as targets and/or projectiles. There were 115 data sets of fixed E and A experiments on which these twenty parameters were allowed to vary while searching for a minimum weighted χ^2. The best values for the parameters were then fit to the polynomials in A and E.

Second, data sets with non-zero $(N - Z)$ dependence were used to adjust thirteen parameters. There were ten parameters held fixed which were the non-asymmetric Woods Saxon potential parameters that had other asymmetric terms within the same term (Eqs. 4,7,11,13,15,18,22,25) and the magic number terms (Eqs. 6,9). There were 90 of these experiment data sets (each data set might contain more than one experiment as detailed above) with some $N - Z$ dependence that were used for this task. The best values for the parameters were then fit to the polynomials in A and E. The parameters that were free to vary in both of these steps were then deduced using an average of both the minimum weighted χ^2 results.

Lastly, the magic number terms were adjusted (Eqs. 6,9) to find the minimum weighted χ^2 within a fixed range keeping everything else fixed. For the magic numbers we used the traditional numbers of 4,8,20, and 28. There were 40 data sets which contained at least one target magic nuclei with both a fixed A and a fixed E which were used to constrain those two parameters.

The variances in the parameters were minimized to a weighted χ^2 which favored forward angles over backward angles (in the χ calculation there was a square root relationship so that the fiftieth forward angle point in a differential cross section was weighted only about one seventh that of the extreme forward point). Differential cross sections were favored over polarizations by a factor of 1.5 and in general neutron total cross section point were favored to be approximately equal to about half of a typical differential cross section. Used, but favored at half the weighting of the total neutron cross section, were the neutron and proton reaction cross sections. We found choosing the correct weightings to be an art form where a balance tenuously existed in which every reaction is counted but certain constraining reactions were strengthen so that the chi squared parameter space contained large relative minimums which our search functions could find easily.

To find the minimum a Monte Carlo search was first done using a Sobol [17] number generator. Since the parameter space was often twenty dimensions this might include up to 3×10^5 vectors in which the weighted χ^2 were calculated at first. Then the lowest ten vectors were analyzed in more detail by looking for local minimums in their vicinity within the χ^2 parameter space. The χ^2 minimization program was a modified Powell program found in Ref. [16]. Although the quality of the fits were examined occasionally, the entire process was close to automatic.

At first the twenty three parameters had large variances which were slowly reduced following the three steps described above as the weighted normalized per point chi-squared was reduced and approached a minimum gracefully. The highest 5% of the χ^2 were thrown out after each fit (which routinely were the same sets) and then each parameter was fit originally to a cubic polynomial in A (nucleon number) and E (projectile energy). Eventually many of the cubics were reduced to quadratics if warranted and in the asymmetry terms the A polynomial was increased to fourth

Proton-Nucleus Experimental Elastic and Total Reaction Data References					
Nucl.	[Ref] (Energies (MeV); Observables)	Nucl.	[Ref] (Energies (MeV); Observables)	Nucl.	[Ref] (Energies (MeV); Observables)
^{12}Be	[19](55;dcs)	^{12}C	[20](20-84;dcs,pol) [21](30;dcs,pol) [24](30-60;rcs) [22](35;dcs) [28](35;dcs) [29](40;dcs) [34](49;dcs) [35](50;dcs) [38](61;dcs) [39](65;dcs,pol) [42](65;rcs) [43](75,150;dcs,pol) [46](81-180;rcs) [47](96,dcs) [49](122,160;dcs,pol) [51](135;dcs,pol,rcs) [54](142;dcs) [55](145;dcs,pol) [31](150;dcs pol) [58](156;dcs,pol)	^{13}C	[21](30;dcs,pol) [22](35;dcs) [25](35;dcs,pol) [30, 31](72;dcs,pol) [36](135;dcs,pol)
^{14}N	[23](30;dcs) [22](35;dcs) [23, 26](50;dcs,pol) [27](35;rcs) [32](122;dcs) [33](142;dcs)				
^{15}N	[22](35;dcs) [37](39,44;dcs) [41](42,44;dcs) [31](65;dcs,pol)			^{16}O	[21](30;dcs,pol) [40](35;dcs,pol) [22, 37](35;dcs) [44](30-47;rcs) [48](43,46;dcs) [26, 35](49;dcs,pol) [52](65;dcs,pol) [42](65;rcs) [56](135;dcs,pol)
^{17}O	[22](35;dcs) [45](66;dcs)				
^{18}O	[22](35;dcs) [41](42,44;dcs) [50](43;dcs) [45](67;dcs)				
^{20}O	[53](30;dcs) [50](43;dcs)				
^{20}Ne	[22](35;dcs) [27](35;rcs) [52](65;dcs,pol)			^{22}O	[57](47;dcs)
				^{22}Ne	[22, 37](35;dcs)
^{24}Mg	[59](30-45;dcs) [60](50;dcs,pol) [39, 52](65;dcs,pol) [63](80;dcs,pol) [64](135;dcs,pol)	^{28}Si*	[61](52;dcs)	^{29}Si	[30](72;dcs,pol)
		^{30}Si	[62](52;dcs)	^{31}P	[30](72;dcs,pol)
		^{32}Si	[65](42;dcs)	^{32}S	[66](53;dcs) [39](65;dcs,pol)
^{34}S	[67](30;dcs)	^{34}Ar	[66](47;dcs)	^{36}Ar	[68](33;dcs)
^{37}Cl	[22, 37](35;dcs)	^{39}K	[22, 37](35;dcs)	^{40}Ar	[69](30,33,37,41;dcs,pol) [22, 23, 37](30-50;dcs,pol) [27](36-47;rcs) [52](65;dcs,pol)
^{40}Ca*	[46](80-180;rcs) [70](30-48;dcs)	^{42}Ar	[68](33;dcs)		
^{42}Ca	[70](30-48;dcs) [71](30-48;rcs) [22](35;dcs) [72](49;dcs) [73](65;dcs,pol)	^{44}Ar	[68](33;dcs)		
		^{44}Ca	[70](30-48;dcs) [71](30-48;rcs) [72](49;dcs) [52, 74](65;dcs,pol)	^{45}Sc	[37](35;dcs) [72](50;dcs,pol)
				^{46}Ti	[52, 73](65;dcs,pol) [75](100;dcs)
^{48}Ca	[70](30-48;dcs) [71](30-48;rcs) [52, 73, 74](65;dcs,pol)	^{48}Ti	[76](30-48;rcs) [52, 73](65;dcs,pol) [75](100;dcs) [77](100;rcs) [58](156;dcs)	^{50}Ti	[73](65;dcs,pol) [75](100;dcs)
				^{50}Cr	[61](52;dcs) [73]
^{52}Cr	[73](65;dcs;pol)			^{54}Cr	[22](35;dcs) [73](65;dcs;pol)
^{54}Fe*	[78](30,40,62;dcs) [80](30-48;rcs) [81](40;dcs,pol)			^{56}Fe*	[24](40,60;rcs) [79](65;dcs,pol)
		^{58}Fe	[22](35;dcs)	^{59}Co	[82](30;dcs) [83](40;dcs) [80](30,40;rcs) [84](65;dcs,pol)

TABLE II: This is a partial listing of the proton-nucleus experimental data used in the fitting process of this work. The rest is located in Table 7 of Ref. [1]. The references are listed followed by the laboratory energy of the projectile and the observables found in the reference (rcs - total reaction cross section, dcs-differential cross section, pol-analyzing power). The data has an energy range from 30 MeV to 160 MeV, and a nucleon number, $12 \leq A \leq 60$. Table 7 of Ref. [1] contains* a substantial listing of experimental data references primarily for the ^{27}Al, ^{28}Si, ^{40}Ca, ^{54}Fe, ^{56}Fe, ^{58}Ni and ^{60}Ni, all those references were used in this work if they were within this optical potentials applicable energy range.

order to give a better fit over the entire nucleon target atomic number range.

B. Experimental Datasets

This work tried strived for a comprehensive collection of experimental data sets. As a starting point we used the excellent summary of elastic data found in Ref. [1], the work of the KD optical potential calculations. We then supplemented this with new data and also nuclei outside the assumed range of the KD potential. These fell within two categories, nuclei lighter than ^{27}Al and those nuclei which are non-spherical and were not considered in that work. There were also a few additional data sets that were discovered and added to our database. All proton-nucleus data sets used that were not in Ref. [1] are listed in Table II. The smaller set of neutron-nucleus data sets used here but not cited in Ref. [1] are listed in Table III. A reader of this work, Ref. [1], and the growing EXFOR/CSISRS database at the *National Nuclear Data Center* [18] have a near complete compilation of elastic nucleon-nucleus and total cross section experimental data at intermediate energies.

Not all the experimental data that exists was used to help constrain the optical potential. Some experimental data, usually published before 1960, had large systematic differences with later data and was disregarded. Also, as

Neutron-Nucleus Experimental Elastic and Total Reaction Data References					
Nucl.	[Ref] (Energies (MeV); Observables)	Nucl.	[Ref] (Energies (MeV); Observables)	Nucl.	[Ref] (Energies; (MeV) Observables)
^{12}C	[85](30-49;rcs) [86](35;dcs)	^{14}N	[85](30-49;rcs)	^{16}O	[85](30-49;rcs) [56](35;dcs)
	[87](55-75;dcs) [88](65-156;dcs)	^{27}Al*	[85](30-49;rcs)	^{28}Si*	[89](misc.;rcs)
	[90](96;dcs) [89, 91](misc.;rcs)	^{40}Ca*	[85](30-49;rcs) [88](65-156;dcs)	^{56}Fe*	[89](misc.;rcs)

TABLE III: This is a partial listing of the neutron-nucleus experimental data used in the fitting process of this work. The rest is located in Table 1 of Ref. [1]. The references are listed followed by the laboratory energy of the projectile and the observables found in the reference (rcs - total reaction cross section, dcs-differential cross section). The data has an energy range from 30 MeV to 160 MeV, and a nucleon number, $12 \leq A \leq 60$ as required by the calculation of this work. Table 1 of Ref. [1] contains* a substantial listing of experimental data references primarily for ^{24}Mg,^{27}Al, ^{28}Si, ^{32}S, ^{40}Ca, and ^{56}Fe, all those reference data sets were also used in this work if they were within this optical potentials applicable energy range. The neutron total cross section data sets of Refs. [92, 93] were also extensively used.

mentioned in Sec. III, calculations were only done if angular differential data existed at a given energy and nucleon number. We felt that total cross section data did not have enough information to fit the parameters accurately so it was only used in conjunction with differential experimental data. Occasionally if the energy of a total cross section was close to an energy where differential data existed, the total reaction cross section data was adjusted following the forms given in Refs. [94, 95]. This procedure was not needed for the total neutron cross section data of Refs. [92, 93] since the energy coverage was substantial for these datasets.

IV. RESULTS

To produce all the calculations shown in this section we used the code TALYS [12, 13] for consistency. All experimental data is shown in black circles, the calculations of this work are shown in light solid green lines (WP), the calculations of Koning and Delaroche [1] (KD) are shown using dark blue dashed lines and the calculations of Madland [2] (MD) used a medium red dot-dashed lines. Our motivation is not to be exhaustive but to give a fair representative overview of the features of these three modern optical potentials. As a global review it can be concluded that that all three potentials do a fairly good job fitting the presently available elastic scattering data and dramatic contrasts are not proffered until section V. The details of this section do illustrate some differences and so we will first proceed first with the neutron-nucleus observables then move to the proton-nucleus observables.

A. Neutron-Nucleus Observables

In Figs. 1-4 we compare the calculations of total neutron cross section results to the comprehensive data sets of Refs. [92, 93]. Overall the calculations of the KD optical potential of Ref. [1] do the best job at reproducing the experimental data, usually within a remarkable 1%. The potential of this work (WP) is usually within 5% of the experimental data sets and that of MD is usually within 10%. These are plotted on an elongated linear scale to accentuate the disparity but it should be recognized that even a 10% difference between theory and experiment is quite small for any nuclear scattering observable.

The remarkable fit by the KD calculation is justified, the authors considered this data important and thus weighted it accordingly. They also had, as discussed in sectionII, a separate proton nucleus and neutron nucleus potential. At energies greater than 50 MeV, where neutron-nucleus elastic scattering data scarce, this was one of the few observables used to fit their neutron optical potential. With fewer constraints this observable, with its high caliber of data [92, 93], was easier to fit. Conversely the optical potential of this work and the optical potential of MD had to continually compromise by both fitting neutron-nucleus and proton-nucleus observables simultaneously.

In Fig. 1 the calculations are fit to four standard nuclei. As in all these calculations the WP calculation of this work (solid green line) was not tested below 30 MeV and the MD calculation was not used below 50 MeV. Likewise the KD calculation is not applicable to the lighter nuclei ($A < 27$) targets as in Fig. 2. Systematic trends emerge where the KD calculation runs lower and closer to the experimental results than the other two calculations for the neutron-nucleus total cross section. The WP calculation is also systematically lower and closer than the MD calculation for the neutron total cross section observables as typified in this figure. There is a small kink in the MD results at $E = 130MeV$, this is a real discontinuity in the Woods Saxon function form parameters for this potential at both 130 MeV and 140 MeV. The history of the phenemological fitting endeavor shows that researchers have struggled to fit these higher

energies well, the present works are no exception.

Fig. 2 contains the lighter targets which follow the same trends as described for Fig. 1. Of the two applicable optical potential calculations the WP optical potential of this work does better in all cases except for neutron scattering from ^{19}F. The odd nuclei have non-zero spin forces which are not included in these optical potentials which in part explain the anomaly.

Concluding our results of neutron-nucleus total cross section calculations are Fig. 3,4 which contain a variety of less common nuclei, and odd spin nuclei neutron total cross sections. The KD optical potential of Ref. [1] which was explicitly not fit to these non-spherical nuclei but still does remarkably well. The same trends discussed in the earlier figures still hold. What becomes apparent in the heavier nuclei ($50 \leq A \leq 60$) calculations of this work (WP - solid green line) is that there seems to be a systematic energy shift; the shape of the curve is good, but it seems to contain a small shift towards higher energies. This could be due to the lack of a coulomb energy correction term in this potential (although a neutron observable, the potential is also fitted simultaneously using proton observables). For remarks on the use and strength of this coulomb correction term see Refs. [1, 4, 7]. Early in the development of this potential we decided to include an asymmetric $N - Z$ adjustment of the short range coulomb radius over the standard coulomb correction terms used in both the KD and MD potentials.

The neutron-nucleus differential experimental data is scarce above 30 MeV (see Table III and Ref. [1]). A representative sample of the data with calculations is shown in Fig. 5. Overall all three potentials describe the experimental data adequately, most impressive are the results of the calculation of the MD potential which simultaneously fits both proton-nucleus and neutron-nucleus data while also using the fewest terms and parameters of the three optical potentials examined. Systematically the WP potential of this work has the weakest results, especially when the scattering angle is greater than 45 degrees This implies that to improve these results the WP potential would need to give more weighting to higher angle results than is now given (see section III). To adequately measure the effects and form of the isospin dependent and asymmetry terms in the optical potential which is used by the WP and MD potentials more high energy neutron-nucleus differential and reaction data is sorely needed [98, 99].

Overall the best optical potential calculation for neutron-nucleus scattering is the work of Koning and Delaroche [1]. It has the best fit to the total cross section observables (even the non-spherical and odd nuclei which were not used to constrain the potential) and it also does an admirable job with the differential observables. It also has a wide energy range and is thus suitable for systematic neutron-nucleus studies. Its largest deficit is that it is not applicable to light nuclei ($A < 27$) which are important in astrophysics and biological physics.

B. Proton-Nucleus Scattering Observables

We move now to the proton-nucleus elastic scattering observables. The potential used by the MD and WP calculations remains the same while the KD potential uses a different optical potential to calculate the proton-nucleus observables.

A representative sample of the inelastic or reaction total cross section data are shown in Fig. 6 over the projectile energy range from 30 MeV to 150 MeV. The calculations in this case are not as close to the experimental data, and the data itself is much sparser and more unsure than the earlier neutron total cross section data. More accurate high energy data is needed in this observable to better constrain the optical model theory (it plays a significant role in determining the absorptive strength)[46, 104]. All three global optical potentials do well but are not excellent. As with the neutron total cross sections the figure is elongated and plotted on a linear scale to emphasis the differences.

There is a much more substantial amount of experimental data for the proton-nucleus differential cross section and analyzing power and we include a representative sample in Figs. 7-13. In Fig. 7 we compare some of the common nuclei targets, ^{27}Al, ^{28}Si, and ^{40}Ca for the differential cross section normalized to the coulomb Rutherford scattering formula. We then examine a heavier common target subset, ^{54,56}Fe and ^{60}N, in Fig. 8. All these nuclei were calculated in Ref. [1] by the KD calculation and in this work are compared with the MD and WP potentials (in the applicable energy ranges, an MD calculation is not created for a kinetic energy of the projectile of less than 50 MeV). Overall all the three calculations do well. Some systematic trends become apparent: the WP potential struggles at the higher angles to reproduce the experimental data (as it did with the neutron-nucleus observables). This miss of the larger angles insinuates that the balance of the weighting functions for the WP potential of this work favored the forward angles too much. The KD potential often exaggerates the minimum which probably signifies that the coulomb force is slightly weak (in general the long term coulomb force mildly obscures the diffraction effect generated by the short term forces). Because these are plotted on a logarithmic scale the percent difference between the theory and experiment is often larger than it initially appears (sometimes as much as 50% compared to 10% for the total cross sections). The quality of fit, as ascertained by an analysis of the χ^2 in Ref. [1], is not as good as with the neutron observables, yet it is still quite impressive for all three optical potentials.

In the next two figures (Fig. 9 and Fig. 10) we examine the reduced differential cross section of target nuclei which

are non-spherical and farther from the line of stability than fit in Ref. [1] using the KD potential. Many are odd, non-spin zero nuclei. Overall the three potentials do surprisingly well with the same systematic problem as with the more popular and common nuclear targets, however some aspects are dissatisfying. In Fig. 9 we show the results of the proton-nucleus reduced differential cross section of the calcium and chromium isotopes and none of the calculations do excellent describing all four isotopes simultaneously. Our research focused on trying to find the strength of the antisymmetry term by simultaneously fitting these isotope's observables together. Our calculation (the solid green line) fit ^{40}Ca and ^{44}Ca isotopes comfortably but struggle with the the other isotopes, the other calculations are in similar predicaments. The general shape is correct but the minimums and maximums are often missed by over 25%. It seems that a asymmetry term which is linear and has mirror symmetry evades accurate discovery. The same difficulties with describing the calcium isotopes were recently discussed in Ref. [98]. These same arguments can be made, to a lesser extent, with chromium. The failure to create an excellent isovector asymmetry term is the motivation for the analysis of section V. It also must be recognized that these potentials are missing a general spin-spin term which may be important for non-spin zero targets. As this potential was being developed a spin-spin term was used but the results had a substantial amount of noise and it was eventually removed. An adequate analysis of the validity and strength of this spin-spin term would be a worthwhile endeavor for future work.

Fig 10 contains the reduced differential cross section of some lighter targets (if $<^{27}$Al the KD calculation is not applicable). This figure shows the struggles the calculations have to fit at higher energies which has been a common problem with an optical model calculation. [49]. In the center panel we highlight some newer differential cross section data of the oxygen isotopes. Our calculation (which is the only one applicable) does well in describing the general trend of the first diffraction minimum shifting as the neutron number increases. The mirror nuclei of calcium and argon are the targets in the right most panel. A recurring disappointment in not being able to fit all the isotopes with the same quality fit, a motivation of this work. However, for those working with exotic beams, this potential does give one a good starting basis for comparison.

In Figs. 11-13 we plot a representative sample of the proton-nucleus spin flip polarization observables. In Fig. 11 we examine tradition nuclear targets, all calculations do well. The calculation of the polarization variable simultaneously with the differential cross section involved an interesting tension between the relative weight of the χ^2 of both observables since the polarization is normalized by the differential cross section. The results show that in many cases our work (the WP potential) fit the polarization better than the differential cross section. In all three polarization figures the major difficulty was again with the lighter nuclei, specifically the carbon isotopes [49, 117] in Figs.12-13. The global optical potential of this work is the best in reproducing this observable over a wide range of targets and chains of nuclei. Additional polarization experimental data is always welcome because it measures the interference between the central and spin-orbit terms and therefore is a good constraint on their relative strengths. The present dataset has a satisfactory amount at projectile energies lower than 100 MeV but more higher energy polarization experiments would be appreciated.

V. ISOVECTOR TERM ANALYSIS

The asymmetry term, that which measures target neutron and proton imbalance, is a point of illustrative comparison and will be the focus of this section to characterize important differences between the optical potentials under examination in this work. Also, the simple linear $N-Z$ dependence of the asymmetric potential has been questioned [8]. We will first examine the validity of this assumption and then follow with the comparison.

A. Validity of $N-Z$

Recently [8], the simple linear $N-Z$ dependence of the asymmetric potential has been tested. All three potentials, following tradition, have used this standard. It is illustrative to use microscopic techniques to develop the optical potential from the nucleon-nucleon potential to examine the origin of this $N-Z$ term. The potential between two nucleons usually contains isospin vector components (usually a spin dependent and a spin independent piece, for simplification here we combine them). Assuming the valid impulse approximation at high energies, we can use the techniques of Kerman, McManus, Thaler [118] and Watson [119, 120] to construct the nucleon-nucleus optical potential from a sum of nucleon-nucleon potentials.

$$V_{asym} \approx \sum_{i}^{A} V_{isoNN}(\tau_{proj} \cdot \tau_i), \tag{27}$$

switching over to raising and lowering operators we can write

$$V_{asym} \approx \sum_{i}^{A} V_{isoNN} \frac{1}{2} (\tau_{proj_+} \tau_{i_-} + \tau_{proj_-} \tau_{i_+} + 2\tau_{proj_z} \tau_{i_z}. \tag{28}$$

If we calculate the difference of the asymmetry piece between the proton projectile and neutron projectile on the same target then microscopically it has this format:

$$V_{asym}(t_{proj} = +\frac{1}{2}) - V_{asym}(t_{proj} = -\frac{1}{2}) \approx V_{isoNN}(\frac{N}{2}\tau_{proj_-} - \frac{Z}{2}\tau_{proj_+} - \frac{N-Z}{4}(\tau_{proj_z}(+\frac{1}{2}) + \tau_{proj_z}(-\frac{1}{2})). \tag{29}$$

The first two terms are inelastic charge exchange terms (the first term is exclusively non-zero for the proton projectile and the second term is non-zero exclusively for the neutron projectile) and the last two terms are the elastic contributions (the same contribution occurs for both the proton or neutron projectile). Notice that a direct $N - Z$ factor is connected to the elastic scattering component. The inelastic term does not contain the equivalent proportionality (the proton potential contains a non-zero N and the neutron potential contains a non-zero negative Z however these potentials are not implemented simultaneously). This does imply that a linear $N - Z$ term in the optical potential, which by definition is both refractive (elastic) and absorptive (inelastic), is simplistic. The imbalance of neutrons to protons does control the physics of the elastic piece, whereas the number of absolute neutrons (for proton scattering) or the number of absolute protons (for neutron scattering) are the source of strength in the inelastic aspect of the optical potential. Although this type of impulse microscopic approximation does not intrinsically contain multiple scattering, correlations, or coupled channels it is a good approximation at higher energies (it has been shown to work adequately at projectile energies of 150 MeV [121]). This microscopic derivation also creates a scattering channel available for direct charge exchange with $N = Z$ nuclei as is verified by experimental evidence with ^{40}Ca as a target [122, 123] for example. The phenemological potentials of this work, with their $N - Z$ asymmetric term, have no outlet for a direct nucleon-nucleon charge exchange reaction and if these reactions are subsumed under another term it would not have an intuitive mechanism to assume a greater neutron or proton nuclear affinity due to an isospin imbalance in the target.

Writing the asymmetric potential in macroscopic nucleon-nucleus optical potential form is also illustrative; we have

$$V_{asym} = V_{isoNA}(\tau_{proj} \cdot \tau_{target}) = V_{isoNA}(\tau_{proj_+}\tau_{target_-} + \tau_{proj_-}\tau_{target_+} + \tau_{proj_z}\tau_{target_z}) \tag{30}$$

and likewise the difference equation subtracting neutron scattering from proton scattering is

$$V_{asym}(t_{proj} = +\frac{1}{2}) - V_{asym}(t_{proj} = -\frac{1}{2}) \approx V_{isoNA}(\tau_{proj_-}\tau_{target_+} - \tau_{proj_+}\tau_{target_-} + \tau_{target_z}). \tag{31}$$

This form again illustrates a direct connection to both elastic scattering and inelastic charge exchange. The elastic z component piece is proportional to $\tau_{target_z} = N - Z$, the inelastic piece is not as concise. In many nuclei the ground state has an isospin vector designation such that τ_{target_z} is the maximum value and thus $|\tau_{target_-}| = |\tau_{target_+}| \propto \sqrt{N-Z}$ but with unstable nuclei this is not always the case and a general rule about the strength of the inelastic piece should be treated with apprehension. All the global optical potentials, because of the linear $N - Z$ term, have trouble giving excellent results for the calcium and chromium isotopes (Fig. 9 and Fig. 10). Similarly, as we explore further from the line of stability it is realized that using a stark absolute linear term leads to erroneous results. For example using a 100 MeV neutron gives physical results when scattering from ^{12,13,14,15}C, but begins to give negative total cross sections for ^{16}C. Obviously, at some point, all elements will return non-physical results when the imbalance between protons and neutrons becomes large. In general the $N - Z$ is a good first approximation, but perhaps a better formulation can be developed.

B. A comparison

We now begin a comparison of the three global optical potentials asymmetry terms. The MD optical potential has a neutron excess asymmetric term for the real volume and the real spin-orbit amplitude only:

$$\mathcal{I}_{MD} = \pm\frac{N-Z}{A} 16.5 f_{WS}(r, \mathcal{R}_i, \mathcal{A}_i) \mp \frac{N-Z}{A} 3.75 \frac{d}{dr} f_{WS}(r, \mathcal{R}_{SO}, \mathcal{A}_{SO})(\mathbf{l} \cdot \sigma) \tag{32}$$

which has no explicit energy dependence and has the standard linear term of $\frac{N-Z}{A}$. The difference between the proton projectile and the neutron projectile is simply a sign change, the internal geometry parameters have no isospin dependence.

The KD optical potential has an explicit asymmetry term only for the real volume component

$$\mathcal{I}_{KD} = \pm\frac{N-Z}{A}21.0(1 - v_2(E-E_f) + v_3(E-E_f)^2 - 7.0e^{-9}(E-E_f)^3)f_{WS}(r,\mathcal{R}_i,\mathcal{A}_i) \tag{33}$$

where v_2 and v_3 are functions which depend on the nucleon number of the target, and projectile energy and the isospin character of the projectile. Likewise E_f represents the Fermi energy of the target, extracted from mass excess values [124], and is dependent on the isospin of the projectile. The internal geometry parameters have no explicit isospin dependence. Because of the separate function dependence on the projectile the asymmetry term,I_{KD} of Eq. 33, is not exactly linear and the isospin flip in the projectile is not simply a sign change as with the I_{MD} term given by Eq. 32.

The optical potential of this work, outlined in Sec. II A, has vector isospin asymmetry $(N-Z)$ in five major terms: real and imaginary volume, imaginary surface, and real and imaginary spin orbit (Eqs. 5,8,12,14,refeq13):

$$\begin{aligned}\mathcal{I}_{WP} = \pm(N-Z)(V_{V_i} + iW_{V_i})f_{WS}(r,\mathcal{R}_i,\mathcal{A}_i) \pm 4(N-Z)\mathcal{A}_S iW_{S_i}\frac{d}{dr}f_{WS}(r,\mathcal{R}_S,\mathcal{A}_S)\\ \pm(N-Z)(V_{SO_i} + iW_{SO_i})\frac{d}{dr}f_{WS}(r,\mathcal{R}_{SO},\mathcal{A}_{SO})\end{aligned} \tag{34}$$

where $V_{V_i}, W_{V_i}, W_{S_i}, V_{SO_i}$, and W_{SO_i} are separable polynomial functions in terms of projectile energy and nucleon number (Eqs. 4-26). There is no projectile isospin dependence within the polynomials. This potential also enforces the separability by using $(N-Z)$ and not $\frac{N-Z}{A}$. We have some explicit asymmetry terms in the $\mathcal{A}_i$ (Eq. 19) and $\mathcal{R}_{SO}$ (Eq. 23) geometry terms which also lead to non-symmetric neutron excess terms. This optical potential has therefore attempted to fit the imaginary volume, surface, and spin orbit asymmetry terms, the other contemporary global optical potentials examined here have set their imaginary asymmetric terms to zero.

To explore this differentiation further let us examine volume integrals which have been illustrative in the past to help describe Gamow-Teller and Fermi charge exchange transitions [125] and to effectively compare the strength of disparate shaped optical potentials. Explicitly we calculate, using the notation of Eq. 2,

$$J_{V_V}/A = -\frac{4\pi}{A}\int_0^\infty r^2\Big(\mathcal{V}_V(E,A,N,Z,MN)\Big)f_{WS}(r,\mathcal{R}_V,\mathcal{A}_V)\,dr \tag{35}$$

$$J_{W_V}/A = -\frac{4\pi}{A}\int_0^\infty r^2 i\Big(\mathcal{W}_V(E,A,N,Z,MN)\Big)f_{WS}(r,\mathcal{R}_V,\mathcal{A}_V)\,dr \tag{36}$$

$$J_{W_S}/A = +\frac{4\pi}{A}4\int_0^\infty r^2\mathcal{A}_S\Big(\mathcal{V}_D(E,A) + i\mathcal{W}_D(E,A,N,Z)\Big)\frac{d}{dr}f_{WS}(r,\mathcal{R}_S,\mathcal{A}_S)\,dr. \tag{37}$$

We will use these equations to examine the differences in volume integrals between a proton projectile and a neutron projectile acting upon the same target nucleus (the isospin asymmetry) and comparing the three optical potentials under study. The difference is emphasized, as it was in the linear study of the $N-Z$ term, because this is what characterizes the isovector asymmetry term from the rest of the dominating isoscalar nuclear potential; it does not disappear. In a well formed neutron and proton global optical potential the asymmetry term is the aspect of the nuclear force which survives an isospin flip in the projectile. In the KD potential, where there are two separate potentials to differentiate proton and neutron scattering, the asymmetry is somewhat ambiguous. Here we will only classify the traditional $\frac{N-Z}{A}$ as the asymmetric term, which we believe is congruent with the design of that potential.

In Fig. 14 the two panels contain results of the real volume integral difference at 50 MeV (left panel) and 150 MeV (right panel) energy for a proton and a neutron projectile for the three global optical potentials. For every nucleon number ($\leq 13A \leq 60$) we have chosen a representative target that is stable or close to the line of stability which are listed in the figure caption. The calculation is explicitly of

$$(ReJ_V/A)_{iso} = (J_{V_V}/A)_{proton} - (J_{V_V}/A)_{neutron}, \tag{38}$$

using the Eqs. 35-37 which shows little agreement at low energies and is even more disparate at higher energies. Likewise at $A < 20$ there is sharp disagreement between the two applicable potentials (MD and WP). This volume integral difference is a direct measure of the change in strength that the three potentials have for the dynamics of a isospin flip of the projectile on the same $N-Z \neq 0$ target. Although the dynamical shape of each curves have similar local minimums and maximums, (this is to be expected because they are similar to Gamow-Teller and Fermi sum rules which are proportional to $N-Z$ [125]), the gross features are wildly different and a valid point of comparison.

The calculation of the imaginary asymmetric potential is a distinct attribute of the WP optical potential described by this work. Calculating the isospin difference of the imaginary term for this potential we have

$$(ImJ_V/A)_{iso} = (J_{W_V}/A - J_{W_S}/A)_{proton} - (J_{W_V}/A - J_{W_S}/A)_{neutron} \tag{39}$$

In Fig. 15 we plot this difference volume integral at a range between 50 MeV and 150 MeV projectile energies. The results are striking, this imaginary volume integral is quite large, often larger than the companion real piece. The imaginary volume integral difference is not monotonic with energy and varies within the filled section of Fig. 15. Having an imaginary asymmetry term allows for a more nuanced optical potential which contains mechanisms for charge exchange resonances [125], important at these energies.

We do believe a comparison of these asymmetric volume integrals differences can me made to experiment. It is well understood that the asymmetry volume integral is tied to GT transitions in charge exchange reactions which dominate at high energies [125]. The volume integral equations of Eqs. 35-39 are equivalent to doing a Fourier transform to momentum transfer (q) space when q=0. With no momentum transfer the inelastic asymmetry terms dominate (in the coulomb distorted wave basis the long range coulomb potential, associated with proton scattering, is external to the optical potential, likewise the neutron scattering elastic forward amplitude is zero). If we take the difference between the energy needed to initiate a proton-neutron charge exchange and a neutron-proton charge exchange for the same target nucleus (the difference in Q values derived from the mass excess values for the resultant final nuclei) this can be compared to the difference in the volume integrals which give the minimum energy, zero momentum transfer, density difference.

Besides including the nuclear asymmetry there is the coulomb potential asymmetry. The volume integral for the coulomb potential is infinite but short range it can easily be defined within the traditional nuclear radius, using the short range expression used by all three potentials when $r < \mathcal{R}_C$, as

$$J_C/A = \frac{4\pi}{A}\int_0^{\mathcal{R}_V\ A^{\frac{1}{3}}} f_{coul}(r, \mathcal{R}_C, A, N, Z) r^2 dr. \tag{40}$$

$$\tag{41}$$

The long range coulomb volume element, which does not converge, should not be included since we work in the distorted wave coulomb basis in which the long range is external to the optical potential. However in the short range it interferes with the nuclear force and thus contribute to the overall strength of the asymmetric volume element. The KD and MD optical potentials also include a coulomb correction term which slightly adds to the depth of the proton real volume term for the KD optical potential and subtracts from the depth of the neutron real volume term for the MD potential. The optical potential of this work (WP) does not contain a coulomb correction term.

To calculate the difference per nucleon in potential energy density at zero momentum transfer we thus follow

$$J_{iso} = (ReJ_V/A + J_{coul.corr./A})_{iso} + (ImJ_V/A)_{iso} + J_C/A - \Delta J_{sr}(q=0) \tag{42}$$

where the first term is from Eq. 38 with the coulomb correction included for the MD and KD potentials. The second and third terms are from Eq. 39 (needed by the WP potential only). and Eq. 40 respectively. The last term is a correction because of the weakening of the Coulomb volume that is used by all three potentials as dictated by Eq. 3. Since the distorted wave basis sets zero nuclear scattering as defined by the traditional long range coulomb form and the short range volume element form used by these potentials is weaker by 20% then the proton zero-scattering point has been shifted lower. The true zeros, within the distorted wave basis of neutron and proton scattering need to be defined consistently when subtracting isospin differences to correctly define the strength of the asymmetry. Thus the correction is

$$\Delta J_{sr}(q=0) = .20 * \frac{4\pi}{A}\int_0^{\mathcal{R}_C\ A^{\frac{1}{3}}} \frac{Ze^2}{r} r^2 dr, \tag{43}$$

which is applied to all the potentials consistently.

In Fig. 16 we plot these Q value differences along with normalized volume integrals for the MD and WP optical potentials for forty-eight different target nuclei at a projectile energy of 150 MeV. The normalized optical potentials were calculated by using Eq. 42 and then multiplying by a constant density. The results are in remarkable agreement. The two optical potentials mimic the shape and structure of the experimental mass excesses, following the global minimum at ^{13}C, local maximums and minimums at ^{39}K and ^{40}K, and the general trends as nucleon number increases. A natural consequence of fitting elastic scattering data with a proton and neutron inclusive optical potential seems to be the ability to fit the Q values of the charge exchange reactions at high energies given a density normalization factor even without this data being used as a fitting constraint. The factor is .38 fm^{-3} for the MD calculation and is .15 fm^{-3} for the WP calculation of this work. The WP density constant is in the right vicinity for nuclear density. The higher MD density factor indicates a weaker asymmetry potential and therefore a quenching of the charge exchange reaction amplitudes. The location of the WP density factor in the right range should not be taken as an indicator that the asymmetry potential is better for the WP calculation since the global optical potential models

Energy MeV	Model	ΔReJ_{iso} MeV fm^3	ΔImJ_{iso} MeV fm^3	$\Delta\sigma_{elast}$ mb	$\Delta\sigma_{react}$ mb	$\Delta\sigma_{tot}$ mb
50	KD	+3.1	0.0	+14	-28	-14
	MD	+32.7	0.0	-36	-9	-45
	WP	+10.8	+8.0	+68	-51	+17
150	KD	+5.5	0.0	-19	-4	-23
	MD	+39.7	0.0	-106	-5	-111
	WP	-0.8	+21.5	+188	-287	-99

TABLE IV: This is a comparison of the strength of the asymmetry term at $A = 40$. The calculation is the difference between neutron-nucleus total cross sections off of ^{40}Ar and ^{40}Ca at two different energies. The differences between the three optical potentials at high energies in the asymmetric term are pronounced and easily separable. At lower energies the differences fall within experimental deviation.

were not constrained by experimental charge exchange data. The KD potential was not included because it does not adequately fit the experimental data because it has separate potentials for the different projectiles. This can be seen by examining Fig. 14 and examining that the KD potential lacks the dynamic extremes of the other two potentials in the asymmetric term and does not come close to describing the local minimums and maximums accurately and so it was not included in the analysis.

We can examine the ramifications of the asymmetric potential differences with reactions that the global optical potentials are constrained to follow. Table IV examines the differences between the ^{40}Ar(n,*) and ^{40}Ca(n,*) cross sections with a 50 and 150 MeV neutron projectile. The large differences generated in the elastic and inelastic cross section predictions are completely dependent on the contrasts in the antisymmetric term between the three potentials. This reaction was chosen because both $A = 40$ nuclei are stable, there are dramatic differences between the potentials at antisymmetric strength at $A = 40$. Using neutrons as projectiles allow a ignorance of coulomb effects. At the 50 MeV projectile energy the differences are not that dramatic and the calculations fall within one standard deviation of experimental error [93, 127] At the higher energy of 150 MeV, where it can be assumed that the born and impulse approximations have validity, the effects of correlations, coupled channels and potential distortions are at a minimum. The dramatic reduction in the inelastic cross section and increase in the elastic cross section predicted by the WP potential differs with the predicted large decrease in the elastic cross section seen by the MD potential. Likewise the KD potential offers a third conclusion; that the differences between ^{40}Ar(n,*) and ^{40}Ca(n,*) cross sections with a 50 and 150 MeV neutron projectile are relatively minor. There is at present no high energy ^{40}Ar(n,*) data to confer which potential is closest to experiment. Experimental results exist (Ref. [128]) which shows a systematic relative weakening of the (n,p) charge exchange compared to the (p,n) when scattering from neutron rich nuclei. Likewise Ref. [129] shows a systematic gain in the (n,p) cross section as more neutrons are added to the target. This would indicate that the (n,p) reaction plays a significantly smaller role in ^{40}Ar(n,*) then in ^{40}Ca(n,*). However charge exchange experiments which exist for the ^{40}Ca target at these high energies do not have full angular coverage to predict an accurate cross section [122, 123] and thus ascertain the strength of charge exchange compared to other inelastic knock-out reactions which are also significant at high energies. Experiments calculating the ^{40}Ar cross sections as in Table IV would be a welcome addition as well as would other high energy neutron data and reaction data like Refs. [46, 104].

VI. CONCLUSION

The motivations for this work were to construct a phenemological nucleon-nucleus global optical potential that is suited to do a wide range of nuclei and energies which will be the tools of the exotic beam accelerators presently running and also under development. We have succeeded in creating one isospin dependent potential which fits target nuclei $12 < A < 60$ and a projectile energy of 30 MeV $<$ 160 MeV. It compares well with two other recent global optical potentials, its advantages are that it is one continuous optical potential which fits all observables well and is designed to do systematic studies on mirror nuclei and chains of isotopes. (files have also been made available to researchers to quickly use this potential for their own use [11]). We have also included an imaginary asymmetry term which is missing from other recent global optical potentials and have given comparative analysis on where these potentials dramatically differ. We also critically examine the validity of the traditional linear proportionality of $N-Z$ in the asymmetry terms. Future work could extend this potential to heavier targets, test other forms of asymmetry potentials and do further work on coming to a good balance between observables. To better constrain the terms with future elastic scattering data from traditional and exotic nuclei we need more data especially at the higher energies.

Acknowledgments

S.P.W. gratefully acknowledges Kirby Keeper, the computing cluster, and the Physics Department at Florida State University for their hospitality during his sabbatical leave where this work was begun. This work was also graciously supported by Eckerd College internal grants which allowed students to work on this project over ensuing summers. We are also indebted to Teragrid grant and extension (PHY060025N) in which a bulk of the computational research was done.

[1] A. J. Koning and J. P. Delaroche, Nucl. Phys. A **713**, 231 (2003).
[2] D. G. Madland, in *Proceedings of OECD/NEA Specialists Meeting on Nucleon-Nucleus Optical Model to 200 MeV* (1997), p. 129, this can also be found at arXiv:nucl-th/9702035v1.
[3] F. D. Becchetti and G. W. Greenlees, Phys. Rev. **182**, 1190 (1969).
[4] J. P. Jeukenne, A. Lejeune, and C. Mahaux, Phys. Rev. C **15**, 10 (1977).
[5] A. Nadasen, P. Schwandt, P. P. Singh, W. W. Jacobs, A. D. Bacher, P. T. Debevec, M. D. Kaitchuck, and J. T. Meek, Phys. Rev. C **23**, 1023 (1981).
[6] R. L. Varner, W. J. Thompson, T. L. McAbee, E. J. Ludwig, and T. B. Clegg, Physics Reports **201**, 57 (1991).
[7] J. Rapaport, V. Kulkarni, and R. W. Finlay, Nucl. Phys. A **330**, 15 (1997).
[8] B. Morillon and P. Romain, Phys. Rev. C **76**, 044601 (2007).
[9] X. Li and C. Cai, Nucl. Phys. A **801**, 43 (2008).
[10] M. A. Melkanoff, T. Sawada, and J. Raynal, in *Methods in Computational Physics* (Academy Press, New York, 1966), vol. VI.
[11] S. P. Weppner, G. Diffendale, and G. Vittorini, *Optical potential calculator*, World Wide Web electronic publication (2008), URL `http://home.eckerd.edu/~weppnesp/optical`.
[12] A. J. Koning, S. Hilaire, and M. C. Duijvestijn, in *Proceedings of International Conference on Nuclear Data for Science and Technology* (AIP, New York, 2004), 769, pp. 1154–1159.
[13] A. J. Koning, S. Hilaire, and M. C. Duijvestijn, *Talys: Comprehensive nuclear reaction modeling*, World Wide Web electronic publication (2008), URL `http://www.talys.eu`.
[14] J. Raynal, Phys. Rev. C. **71**, 057602 (2005), and references within.
[15] A. R. Barnett, Comp. Phys. Comm. **27**, 147 (1982).
[16] W. Press, B. Flannery, S. Teukolsky, and W. Vetterling, *Numerical Recipes in FORTRAN: The Art of Scientific Computing, 2nd Ed.* (Cambridge University Press, Cambridge, England, 1992), chap. 10.
[17] P. Bratley and B. Fox, ACM Trans. on Math. Soft. **14**, 88 (1988).
[18] *National nuclear data center*, World Wide Web electronic publication (2008), URL `http://www.nndc.bnl.gov`.
[19] A. A. Korsheninnikov, E. Y. Nikolskii, T. Kobayashi, D. V. Aleksandrov, M. Fujimaki, H. Kumagai, A. A. Ogloblin, A. Ozawa, I. Tanihata, Y. Watanabe, et al., Phys. Lett. B **343**, 53 (1995).
[20] M. Ieiri, H. Sakaguchi, M. Nakamura, H. Sakamoto, H. Ogawa, M. Yosoi, T. Ichihara, N. Isshiki, Y. Takeuchi, H. Togawa, et al., Nucl. Instrum. Methods in Phys. Res. Sect A. **257**, 253 (1987).
[21] P. D. Greaves, V. Hnizdo, J. Lowe, and O. Karban, Nucl. Phys. A **179**, 1 (1972).
[22] E. Fabrici, S. Micheletti, M. Pignanelli, F. G. Resmini, R. De Leo, G. D'Erasmo, and A. Pantaleo, Phys. Rev. C **21**, 844 (1980).
[23] A. A. Rush, E. J. Burge, and D. A. Smith, Nucl. Phys. A **166**, 378 (1971).
[24] J. J. Menet, E. E. Gross, J. J. Malanify, and A. Zucker, Phys. Rev. C **4**, 1114 (1971).
[25] H. Ohnuma, B. A. Brown, D. Dehnhard, K. Furukawa, T. Hasegawa, S. Hayakawa, N. Hoshino, K. Ieki, M. Kabasawa, K. Maeda, et al., Nucl. Phys. A **456**, 61 (1986).
[26] N. M. Clarke, E. J. Burge, and D. A. Smith, Nucl. Phys. A **157**, 145 (1970).
[27] R. F. Carlson, A. J. Cox, T. N. Nasr, M. S. D. Jong, D. L. Ginther, D. K. Hasell, A. M. Sourkes, W. T. H. V. Oers, and D. J. Margaziotis, Nucl. Phys. A **445**, 57 (1985).
[28] M. Pignanelli, S. Micheletti, R. De Leo, S. Brandenburg, and M. N. Harakeh, Phys. Rev. C **33**, 40 (1986).
[29] L. N. Blumberg, E. E. Gross, A. V. der Woude, A. Zucker, and R. H. Bassel, Phys. Rev. **147**, 812 (1966).
[30] B. V. Przewoski, P. D. Eversheim, F. Hinterberger, U. Lahr, J. Campbell, J. Gtz, M. Hammans, R. Henneck, G. Masson, , et al., Nucl. Phys. A **528**, 159 (1991).
[31] V. M. Hannen, K. Amos, A. M. van den Berg, R. K. Bieber, P. K. Deb, F. Ellinghaus, D. Frekers, M. Hagemann, M. N. Harakeh, J. Heyse, et al., Phys. Rev. C **67**, 054321 (2003).
[32] J. R. Comfort, S. M. Austin, P. T. Debevec, G. L. Moake, R. W. Finlay, and W. G. Love, Phys. Rev. C **21**, 2147 (1980).
[33] A. E. Taylor and E. Wood, Nucl. Phys. **25**, 642 (1961).
[34] V. I. Grancev, V. I. Konfederatenko, V. A. Kornilov, O. F. Nemec, , R. G. Rudenko, M. V. Sokolov, and B. G. Struzhko, U.F.Z. **28**, 506 (1983).
[35] J. A. Fannon, E. J. Burge, D. A. Smith, and N. K. Ganguly, Nucl. Phys. A **97**, 263 (1967).
[36] S. F. Collins, G. G. Shute, B. M. Spicer, V. C. Officer, I. Morrison, K. A. A. D. W. Devins, D. L. Friesel, and W. P. Jones, Nucl. Phys. A **380**, 445 (1982).
[37] E. Colombo, R. D. Leo, J. L. Escudie, E. Fabrici, S. Micheletti, M. Pignanelli, and F. Resmini, J. Phys. Soc. Japan Suppl. **44**, 543 (1978).
[38] C. B. Fulmer, J. B. Ball, A. Scott, and M. L. Whitten, Phys. Rev. **181**, 1565 (1969).
[39] S. Kato, K. Okada, M. Kondo, K. Hosono, T. Saito, N. Matsuoka, K. Hatanaka, T. Noro, S. Nagamachi, H. Shimizu, et al., Phys. Rev. C **31**, 1616 (1985).
[40] H. Ohnuma, N. Hoshino, K. Ieki, M. Iwase, H. Shimizu, H. Toyokawa, T. Hasegawa, K. Nisimura, M. Yasue, H. Kabasawa, et al., Nucl. Phys. A **514**, 273 (1990).
[41] E. Fabrici, S. Micheletti, M. Pignanelli, F. G. Resmini, R. De Leo, G. D'Erasmo, A. Pantaleo, J. L. Escudié, and A. Tarrats, Phys. Rev. C **21**, 830 (1980).

[42] A. Ingemarsson, J. Nyberg, P. U. Renberg, O. Sundberg, R. F. Carlson, A. Auce, R. Johansson, G. Tibell, B. C. Clark, L. K. Kerr, et al., Nucl. Phys. A **653**, 341 (1999).
[43] C. Rolland, B. Geoffrion, N. Marty, M. Morlet, B. Tatischeff, and A. Willis, Nucl. Phys. **80**, 625 (1966).
[44] R. F. Carlson, A. J. Cox, J. R. Nimmo, N. E. Davison, S. A. Elbakr, J. L. Horton, A. Houdayer, A. M. Sourkes, W. T. H. van Oers, and D. J. Margaziotis, Phys. Rev. C **12**, 1167 (1975).
[45] G. M. Lerner and J. B. Marion, Nucl. Phys. A **193**, 593 (1972).
[46] A. Auce, A. Ingemarsson, R. Johansson, M. Lantz, G. Tibell, R. F. Carlson, M. J. Shachno, A. A. Cowley, G. C. Hillhouse, N. M. Jacobs, et al., Phys. Rev. **C71**, 064606 (2005).
[47] K. Strauch and F. Titus, Phys. Rev. **103**, 200 (1956).
[48] J. M. Cameron, J. R. Richardson, W. T. H. V. Oers, and J. W. Verba, Phys. Rev. **167**, 908 (1968).
[49] H. O. Meyer, P. Schwandt, W. W. Jacobs, and J. R. Hall, Phys. Rev. C **27**, 459 (1983).
[50] E. Khan, Y. Blumenfeld, N. V. Giai, T. Suomijarvi, N. Alamanos, F. Auger, G. Colo, N. Frascaria, A. Gillibert, T. Glasmacher, et al., Phys. Lett. B **490**, 45 (2000).
[51] W. Bauhoff, S. F. Collins, R. S. Henderson, G. G. Shute, B. M. Spicer, V. C. Officer, K. A. Amos, I. Morrison, D. W. Devins, D. L. Friesel, et al., Nucl. Phys. A **410**, 180 (1983).
[52] H. Sakaguchi, M. Nakamura, K. Hatanaka, A. Goto, T. Noro, F. Ohtani, H. Sakamoto, H. Ogawa, and S. Kobayashi, Phys. Rev. C **26**, 944 (1982).
[53] J. K. Jewell, L. A. Riley, P. D. Cottle, K. W. Kemper, T. Glasmacher, R. W. Ibbotson, H. Scheit, M. Chromik, Y. Blumenfeld, S. E. Hirzebruch, et al., Phys. Lett. B **454**, 181 (1999).
[54] A. E. Taylor and E. Wood, Nucl. Phys. **25**, 642 (1961).
[55] J. M. Emmerson, J. C. W. Madden, C. M. P. Johnson, N. Middlemas, A. B. Clegg, and W. S. C. Williams, Nucl. Phys. **77**, 305 (1966).
[56] J. J. Kelly, W. Bertozzi, T. N. Buti, J. M. Finn, F. W. Hersman, C. Hyde-Wright, M. V. Hynes, M. A. Kovash, B. Murdock, B. E. Norum, et al., Phys. Rev. C **39**, 1222 (1989).
[57] E. Becheva, Y. Blumenfeld, E. Khan, D. Beaumel, J. M. Daugas, F. Delaunay, C. E. Demonchy, A. Drouart, M. Fallot, A. Gillibert, et al., Phys. Rev. Lett. **96**, 012501 (2006).
[58] V. Comparat, R. Frascaria, N. Marty, M. Morlet, and A. Willis, Nucl. Phys. A **221**, 403 (1974).
[59] D. K. Hasell, N. E. Davison, T. N. Nasr, B. T. Murdoch, A. M. Sourkes, and W. T. H. V. Oers, Phys. Rev. C **27**, 482 (1983).
[60] A. A. Rush, E. J. Burge, V. E. Lewis, D. A. Smith, and N. K. Ganguly, Nucl. Phys. A **104**, 340 (1967).
[61] H. Ohnuma, J.Kasagi, F.Kakimoto, S.Kubono, and K.Koyama, J. Phys. Soc. Japan **48**, 1812 (1980).
[62] N. Alamanos, A. Pakou, A. Lagoyannis, and A. Musumarra, Nucl. Phys. A **660**, 406 (1999).
[63] K. Hatanaka, M. Fujiwara, K. Hosono, N. Matsuoka, T. Saito, and H. Sakai, Phys. Rev. C **29**, 13 (1984).
[64] P. Schwandt, H. O. Meyer, W. W. Jacobs, A. D. Bacher, S. E. Vigdor, M. D. Kaitchuck, and T. R. Donoghue, Phys. Rev. C **26**, 55 (1982).
[65] P. D. Cottle, Z. Hu, B. V. Pritychenko, J. A. Church, M. Fauerbach, T. Glasmacher, R. W. Ibbotson, K. W. Kemper, L. A. Riley, H. Scheit, et al., Phys. Rev. Lett. **88**, 172502 (2002).
[66] E. Khan, T. Suomijarvi, Y. Blumenfeld, V. G. Nguyen, N. A. amd F. Auger, E. Bauge, D. Beaumel, J. P. Delaroche, P. Delbourgo-Salvador, and A. Drouart, Nucl. Phys. A **694**, 103 (2001).
[67] R. Alarcon, J. Rapaport, R. T. Kouzes, W. H. Moore, and B. A. Brown, Phys. Rev. C **31**, 697 (1985).
[68] H. Scheit, F. Maréchal, T. Glasmacher, E. Bauge, Y. Blumenfeld, J. P. Delaroche, M. Girod, R. W. Ibbotson, K. W. Kemper, J. Libert, et al., Phys. Rev. C **63**, 014604 (2000).
[69] N. T. Okumusoglu, J. Birchall, M. S. A. L. Al-Ghazi, C. Lapointe, J. S. C. Mckee, H. E. Conzett, R. M. Larimer, and P. Von-Rossen, Nucl. Phys. A **393**, 45 (1983).
[70] R. H. McCamis, T. N. Nasr, J. Birchall, N. E. Davison, W. T. H. V. Oers, P. J. T. Verheijen, R. F. Carlson, A. J. Cox, B. C. Clark, E. D. Cooper, et al., Phys. Rev. C **33**, 1624 (1986).
[71] R. F. Carlson, A. J. Cox, N. E. Davison, T. Eliyakut-Roshko, R. H. Mccamis, and W. T. H. V. Oers, Phys. Rev. C **49**, 3090 (1994).
[72] G. S. Mani, D. T. Jones, and D. Jacques, Nucl. Phys. A **165**, 384 (1971).
[73] T. Noro, H. Sakagochi, M. Nakamura, K. Natanaka, F. Ohtani, H. Sakamoto, and S. Kobayashi, Nucl. Phys. A **366**, 189 (1989).
[74] H. Sakaguchi, Memoirs Faculty of Sci., Kyoto Univ.,Ser.Phys. **36**, 305 (1982).
[75] L. W. Woo, N. S. Wall, P. G. Roos, P. H. Debenham, K. Kwiatkowski, and A. Nadasen, Phys. Rev. C **29**, 794 (1984).
[76] T. N. Nasr, A. M. Sourkes, D. J. Margaziotis, R. L. Carlson, and A.J.Cox, Can. Jour. Phys. **56**, 56 (1978).
[77] R. F. Carlson, At. Data Nucl. Data Tables **63**, 93 (1996).
[78] F. E. Bertrand and R. W. Peelle, Phys. Rev. C **8**, 1045 (1973).
[79] R. De Leo, H. Akimune, N. Blasi, I. Daito, Y. Fujita, M. Fujiwara, S. I. Hayakawa, S. Hatori, K. Hosono, H. Ikegami, et al., Phys. Rev. C **53**, 2718 (1996).
[80] R. H. McCamis, N. E. Davison, W. T. H. V. Oers, R. F. Carlson, and A. J. Cox, Jour. Can. Phys. **64**, 685 (1986).
[81] M. P. Fricke, E. E. Gross, and A. Zucker, Phys. Rev. **163**, 1153 (1967).
[82] B. W. Ridley and J. F. Turner, Nucl. Phys. **58**, 497 (1964).
[83] M. P. Fricke, E. E. Gross, B. J. Morton, and A. Zucker, Phys. Rev. **156**, 1207 (1967).
[84] H. Sakaguchi, M. Nakamura, K. Hatanaka, T. Noro, F. Ohtani, H. Sakamoto, H. Ogawa, and S. Kobayashi, Phys. Lett. **B99**, 92 (1981).

[85] P. Dimbylow, Physics in Medicine and Biology **25**, 637 (1980).
[86] T. Niizeki, H. Orihara, K. Ishii, K. Maeda, M. Kabasawa, Y. Takahashi, and K. Miura, Nucl. Inst. Meth. Phys. Res. A **287**, 455 (1990).
[87] M. Ibaraki, M. Baba, T. Miura, Y. Hirasawa, Y. Nauchi, H. Nakashima, S. I.Meigo, S. T. O. Iwamoto, N. Hirakawa, and T. Hiroishi, Nucl.Science and Technol.Tokyo,Supplement **2**, 204 (2002).
[88] J. H. Osborne, F. P. Brady, J. L. Romero, J. L. Ullmann, D. S. Sorenson, A. Ling, N. S. P. King, R. C. Haight, J.Rapaport, R. W. Finlay, et al., Phys. Rev. C **70**, 054613 (2004).
[89] K. Amos and S. Karataglidis, Phys. Rev. C **65**, 057603 (2002).
[90] J. Klug, J. Blomgren, A. Ataç, B. Bergenwall, A. Hildebrand, C. Johansson, P. Mermod, L. Nilsson, S. Pomp, U. Tippawan, et al., Phys. Rev. C **68**, 064605 (2003).
[91] P. K. Deb, K. Amos, S. Karataglidis, M. B. Chadwick, and D. G. Madland, Phys. Rev. Lett. **86**, 3248 (2001).
[92] R. W. Finlay, W. P. Abfalterer, G. Fink, E. Montei, T. Adami, P. W. Lisowski, G. L. Morgan, and R. C. Haight, Phys. Rev. C **47**, 237 (1993).
[93] W. P. Abfalterer, F. B. Bateman, F. S. Dietrich, R. W. Finlay, R. C. Haight, and G. L. Morgan, Phys. Rev. C **63**, 044608 (2001).
[94] K. Amos, S. Karataglidis, and P. K. Deb, Phys. Rev. C **65**, 064618 (2002).
[95] P. K. Deb and K. Amos, Phys. Rev. C **69**, 064608 (2004).
[96] R. W. Finlay, W. P. Abfalterer, G. Fink, E. Montei, T. Adami, P. W. Lisowski, G. L. Morgan, and R. C. Haight, Phys. Rev. C **47**, 237 (1993).
[97] W. P. Abfalterer, F. B. Bateman, F. S. Dietrich, R. W. Finlay, R. C. Haight, and G. L. Morgan, Phys. Rev. C **63**, 044608 (2001).
[98] R. J. Charity, J. M. Mueller, L. G. Sobotka, and W. H. Dickhoff, Phys. Rev. C **76**, 044314 (2007).
[99] A. Öhrn, J. Blomgren, P. Andersson, A. Ataç, C. Gustavsson, J. Klug, P. Mermod, S. Pomp, P. Wolniewicz, M. Österlund, et al., Physical Review C (Nuclear Physics) **77**, 024605 (pages 11) (2008), URL `http://link.aps.org/abstract/PRC/v77/e024605`.
[100] R. P. Devito, S. M. Austin, U. E. B. Berg, R. Deleo, and W. A. Sterrenburg, Phys. Rev. **C28**, 2530 (1983).
[101] E. L. Hjort, F. P. Brady, J. R. Drummond, B. McEachern, J. H. Osborne, J. L. Romero, D. S. Sorenson, and H. H. K. Tang, Phys. Rev. C **53**, 237 (1996).
[102] R. P. Devito, S. M. Austin, W. Sterrenburg, and U. E. P. Berg, Phys. Rev. Lett. **47**, 628 (1981).
[103] E. L. Hjort, F. P. Brady, J. L. Romero, J. R. Drummond, D. S. Sorenson, J. H. Osborne, B. McEachern, and L. F. Hansen, Phys. Rev. C **50**, 275 (1994).
[104] B. Abu-Ibrahim, W. Horiuchi, A. Kohama, and Y. Suzuki, Physical Review C (Nuclear Physics) **77**, 034607 (pages 11) (2008), URL `http://link.aps.org/abstract/PRC/v77/e034607`.
[105] F. E. Bertrand and R. W. Peelle, Phys. Rev. C **8**, 1045 (1973).
[106] A. E. Taylor and E. Wood, Nucl. Phys. **25**, 642 (1961).
[107] C. Olmer, A. D. Bacher, G. T. Emory, W. P. Jones, D. W. Miller, H. Nann, P. Schwandt, S. Y. T. E. Drake, and R. J. Sobie, Phys. Rev. C **29**, 361 (1984).
[108] E. Bauge, J. P. Delaroche, and M. Girod, Phys. Rev. C **58**, 1118 (1998).
[109] H. S. Liers, R. N. Boyd, C. H. Poppe, J. A. Sievers, and D. L. Watson, Phys. Rev. C **2**, 1399 (1970).
[110] K. Kwiatkowski and N. S. Wall, Nucl. Phys. A **301**, 349 (1978).
[111] P. G. Roos and N. S. Wall, Phys. Rev. B **140**, 1237 (1965).
[112] Y. Blumenfeld, E. Khan, F. Maréchal, and T. Suomijarvi, Pramana J. Phys. **57**, 493 (2001).
[113] L. N. Blumberg, E. E. Gross, A. V. D. Woude, A. Zucker, and R. H. Bassel, Phys. Rev. **147**, 812 (1966).
[114] R. M. Craig, J. C. Dore, J. Lowe, and D. L. Watson, Nucl. Phys. **86**, 113 (1966).
[115] V. Hnizdo, O. Karban, J. Lowe, G. W. Greenlees, and W. Makofske, Phys. Rev. C. **3**, 1560 (1971).
[116] G. W. Greenlees, V. Hnizdo, O. Karban, J. Lowe, and W. Makofske, Phys. Rev. C **2**, 1063 (1970).
[117] P. K. Deb and K. Amos, Phys. Rev.C **62**, 024605 (2000).
[118] A. Kerman, M. McManus, and R. M. Thaler, Ann. Phys. **8**, 551 (1959).
[119] K. M. Watson, Phys. Rev. **89**, 575 (1953).
[120] N. C. Francis and K. M. Watson, Phys. Rev. **92**, 291 (1953).
[121] K. Amos, P. J. Dortmans, H. V. Geramb, S. Karataglidis, and J. Raynal, in *Advances in Nuclear Physics, Vol. 25*, edited by J. W. Negele and E. Vogt (Plenum Publishers, New York, 2000), and references within.
[122] B. K. Park, J. Rapaport, J. L. Ullmann, A. G. Ling, D. S. Sorenson, F. P. Brady, J. L. Romero, C. R. Howell, W. Tornow, and C. T. Rönnqvist, Phys. Rev. C **45**, 1791 (1992).
[123] C. Hautala, J. Rapaport, M. Palarczyk, D. L. Prout, D. A. Cooper, G. Savopulos, B. Anderson, A. Baldwin, C. C. Foster, C. D. Goodman, et al., Phys. Rev. C **65**, 034612 (2002).
[124] G. Audi and A. H. Wapstra, Nucl. Phys. A **595**, 409 (1995).
[125] F. Osterfeld, Rev. Mod. Phys. **64**, 491 (1992).
[126] G. Audi, A. H. Wapstra, and C. Thibault, Nucl. Phys. A **729**, 337 (2006).
[127] R. R. Winters, R. F. Carlton, C. H. Johnson, N. W. Hill, and M. R. Lacerna, Phys. Rev. C **43**, 492 (1991).
[128] M. B. Aufderheide, S. D. Bloom, D. A. Resler, and G. J. Mathews, Phys. Rev. C **48**, 1677 (1993).
[129] K. P. Jackson, A. Celler, W. P. Alford, K. Raywood, Q. Abegg, R. E. Azuma, C. K. Campbell, S. ElKateb, D. Frekers, P. W. Green, et al., Phys. Lett. B **201**, 25 (1988).

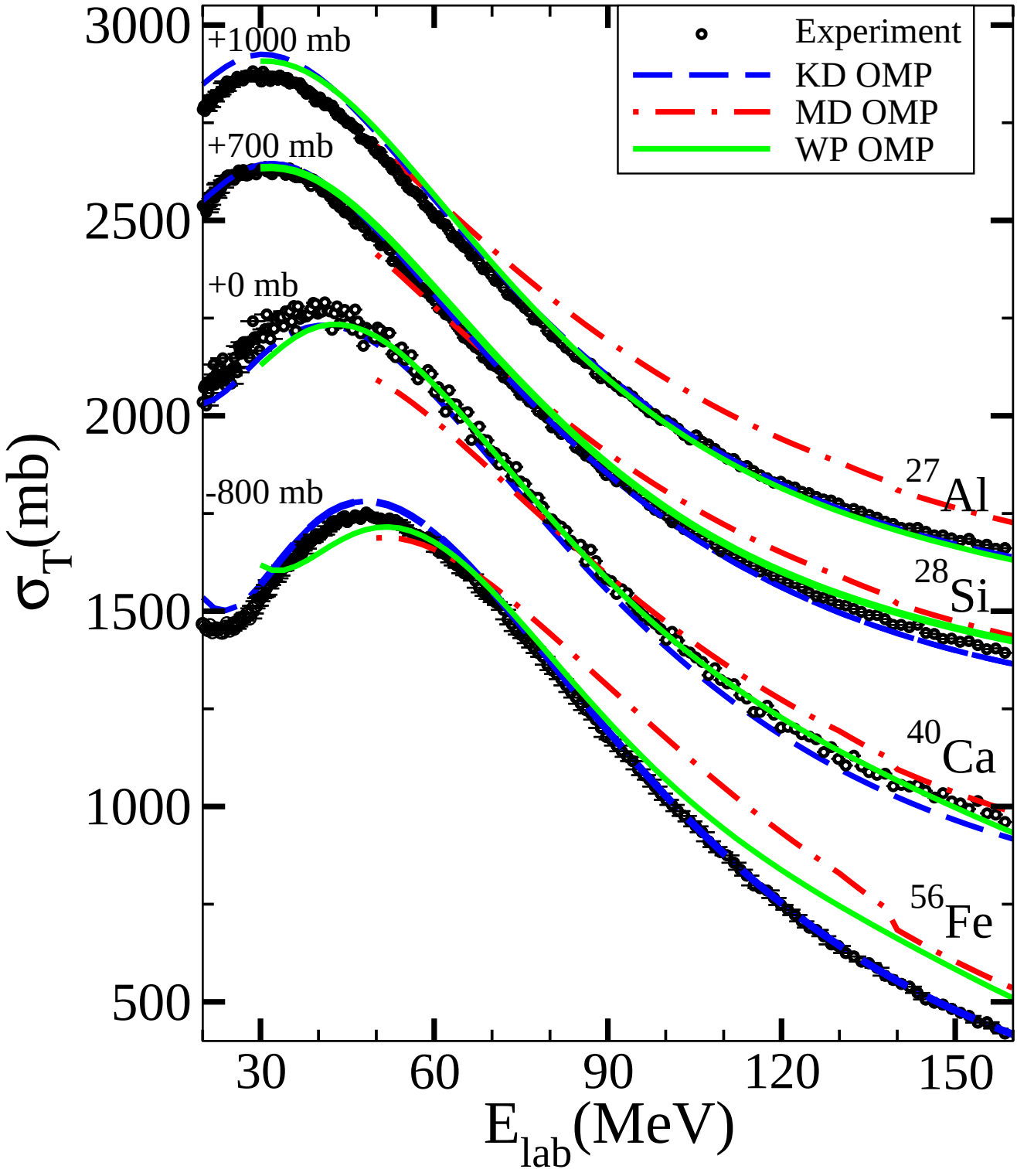

FIG. 1: The experimental total cross section for neutrons scattering from ^{27}Al[96],^{28}Si[96],^{40}Ca[97] and ^{56}Fe[97] from 20 MeV to 160 MeV for the laboratory energy of the neutron. They are fit to three different optical potential calculations (KD[1],MD[2] and to this work: WP) which are described in the legend. The experimental data and theory have been offset by constant amounts for multiple comparisons on one graph. The WP and MD calculations have a minimum energy limit of 30 and 50 MeV respectively.

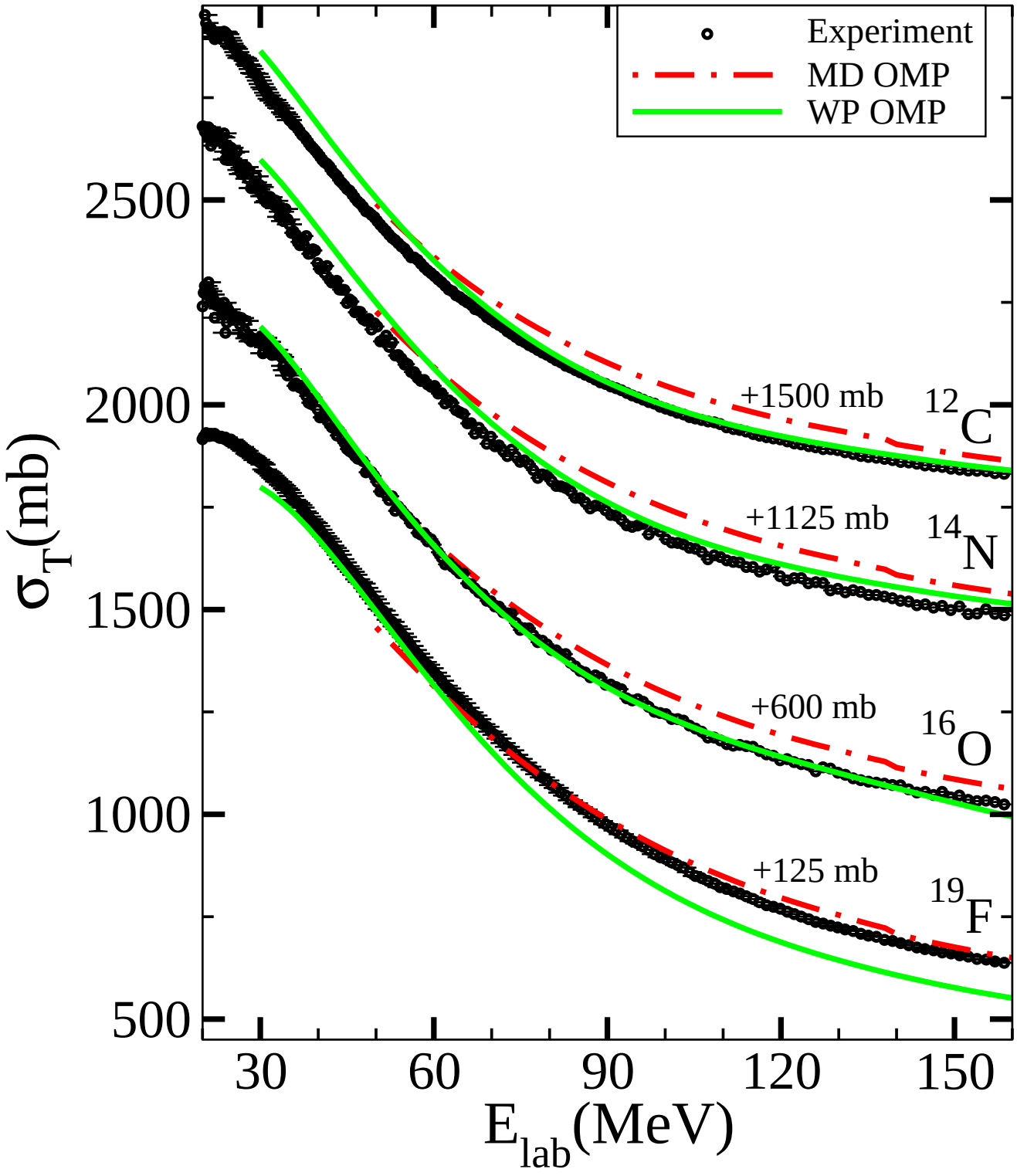

FIG. 2: The experimental total cross section for neutrons scattering from the light nuclei of ^{12}C[97],^{14}N[96],^{16}O[96] and ^{19}F[97] from 20 MeV to 160 MeV for the laboratory energy of the neutron. They are fit to two different optical potential calculations (MD[2] and to this work: WP) which are described in the legend. The experimental data and theory have been offset by constant amounts for multiple comparisons on one graph. The WP and MD calculations have a minimum energy limit of 30 and 50 MeV respectively. The KD calculation is not applicable for these light nuclei.

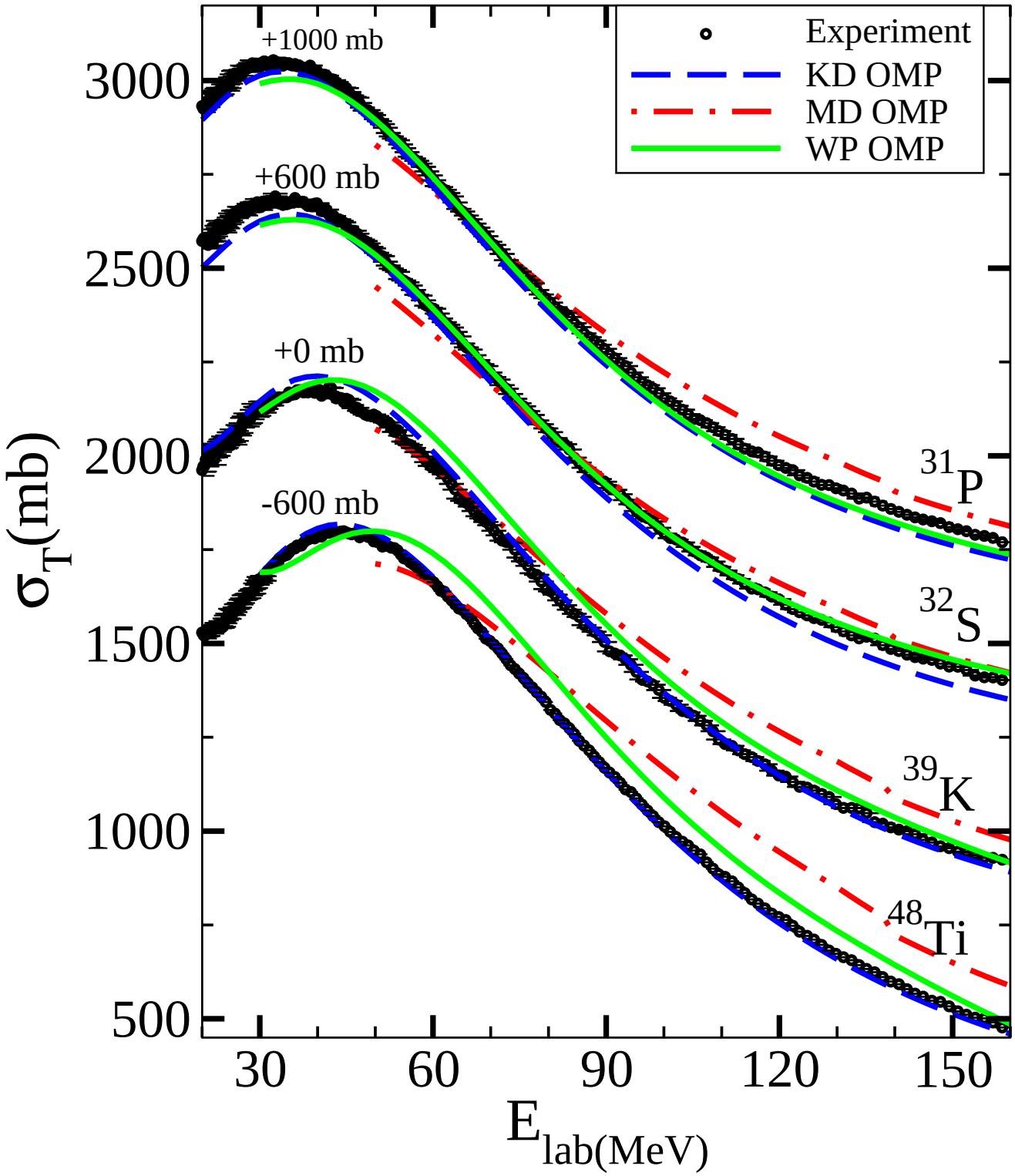

FIG. 3: The experimental total cross section for neutrons scattering from ^{31}P[97],^{32}S[97],^{39}K[97] and ^{48}Ti[97] from 20 MeV to 160 MeV for the laboratory energy of the neutron. They are fit to three different optical potential calculations (KD[1],MD[2] and to this work: WP) which are described in the legend. The experimental data and theory have been offset by constant amounts for multiple comparisons on one graph. The WP and MD calculations have a minimum energy limit of 30 and 50 MeV respectively.

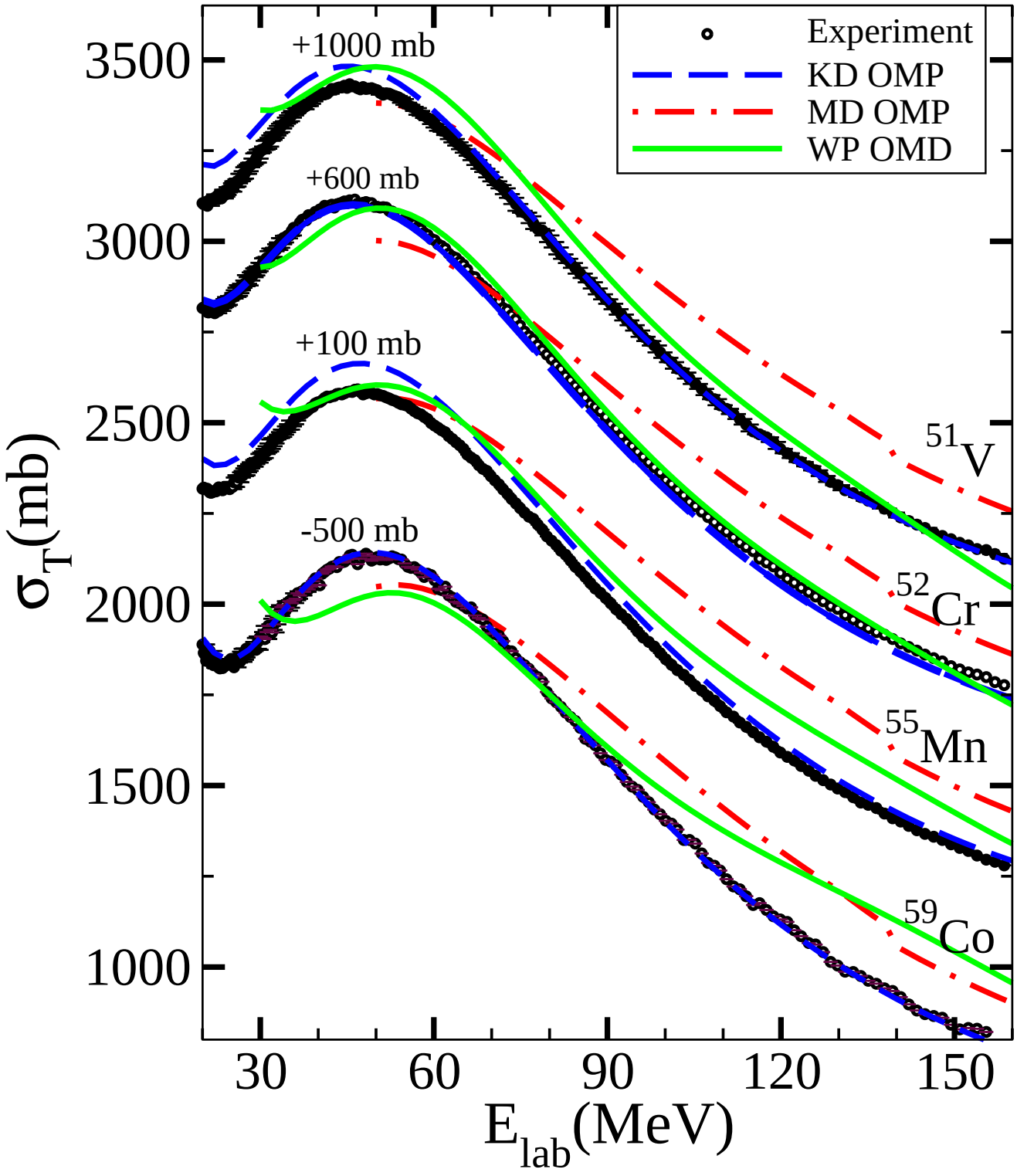

FIG. 4: The experimental total cross section for neutrons scattering from ^{51}V[97],^{52}Cr[97],^{55}Mn[97] and ^{59}Co[97] from 20 MeV to 160 MeV for the laboratory energy of the neutron. They are fit to three different optical potential calculations (KD[1],MD[2] and to this work: WP) which are described in the legend. The experimental data and theory have been offset by constant amounts for multiple comparisons on one graph. The WP and MD calculations have a minimum energy limit of 30 and 50 MeV respectively.

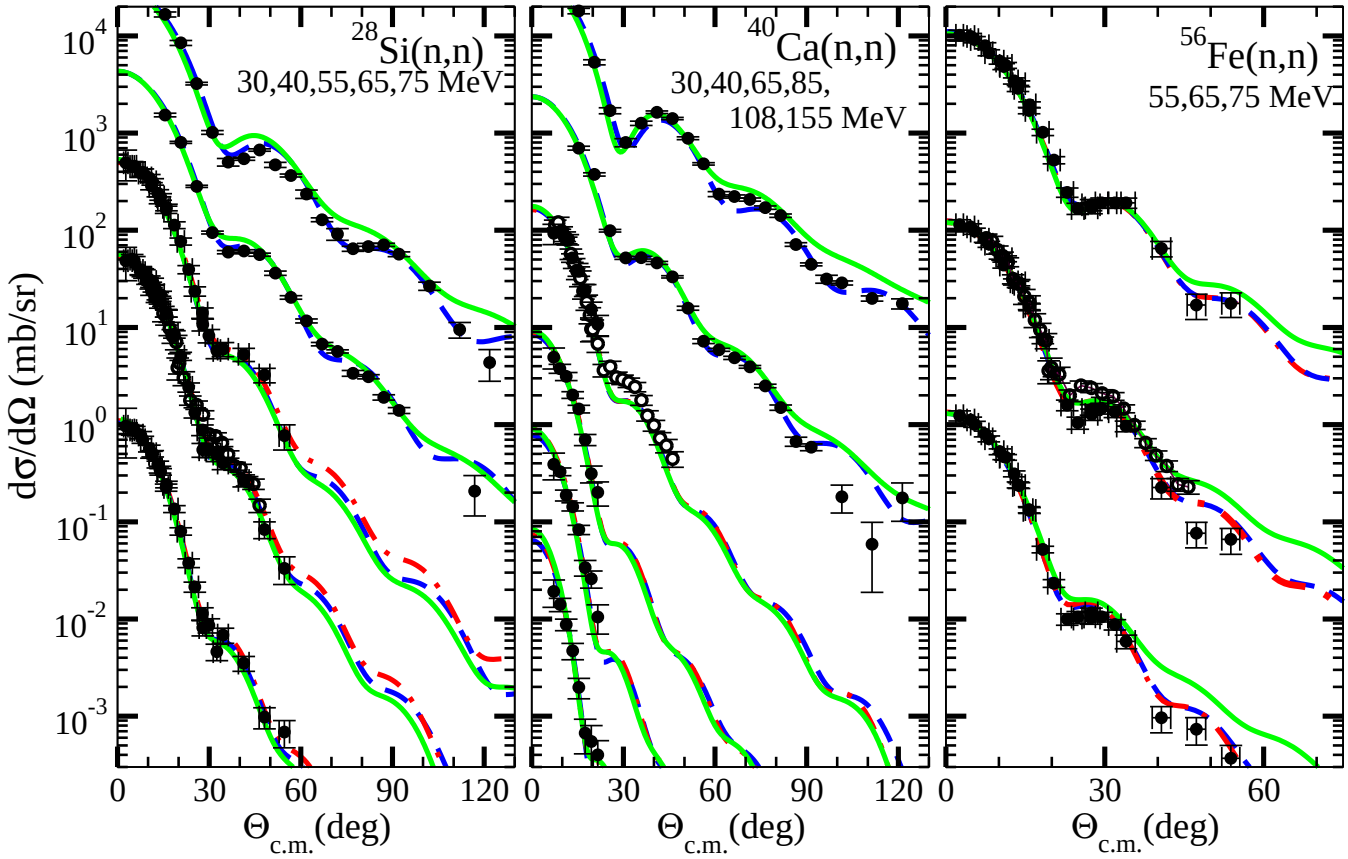

FIG. 5: Neutron-nucleus elastic differential cross section experimental data for the target nuclei of ^{28}Si[87, 100, 101], ^{40}Ca[88, 101, 102], ^{56}Fe[87, 100, 101, 103] at a variety of incident laboratory energies. They are fit to three different optical potential calculations (KD[1],MD[2] and to this work: WP). As in all figures, KD is a dashed line, MD is a dot-dashed line and WP is a solid line. The experimental data and theory have been offset by constant amounts for multiple comparisons on one graph. The MD calculations has a minimum energy limit of 50 MeV and is therefore missing from calculations below that energy.

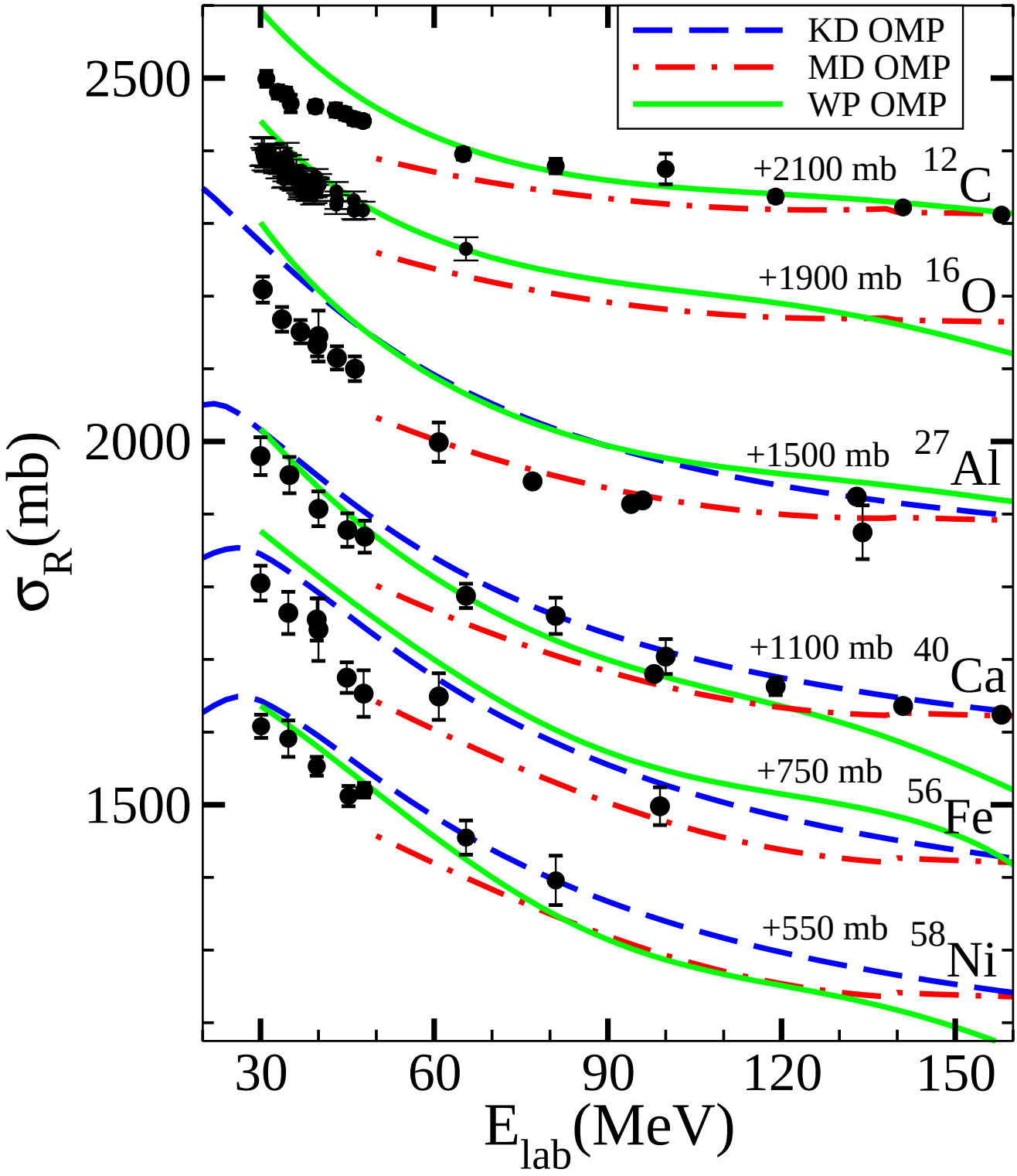

FIG. 6: Proton-nucleus total inelastic cross section data for the targets ^{12}C,^{16}O, ^{27}Al,^{40}Ca, ^{56}Fe, and ^{58}Ni from 20 MeV to 160 MeV for the laboratory energy of the projectile proton. The experimental data comes from a variety of sources and are compiled and discussed in Refs. [1, 77, 94]. There are also new higher energy measurements for ^{12}C and ^{40}Ca found in Ref. [46]. They are fit to three different optical potential calculations (KD[1],MD[2] and to this work: WP) which are described in the legend. The experimental data and theory have been offset by constant amounts for multiple comparisons on one graph. The WP and MD calculations have a minimum energy limit of 30 and 50 MeV respectively.

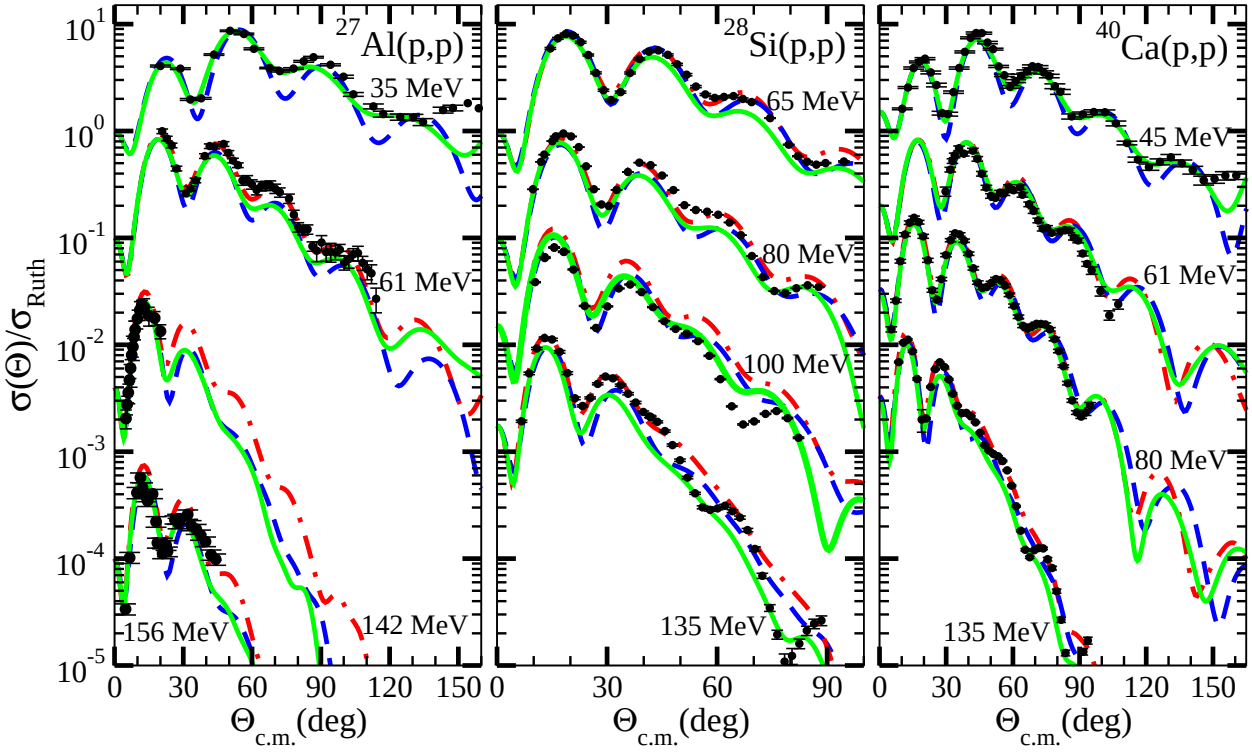

FIG. 7: Proton-nucleus elastic Rutherford reduced differential cross section experimental data for the target nuclei of ^{27}Al[37, 38, 58, 105, 106], ^{28}Si[42, 107], ^{40}Ca[5, 38, 70], at varying proton laboratory energies. Refer to Fig. 5 for details of the theoretical calculations.

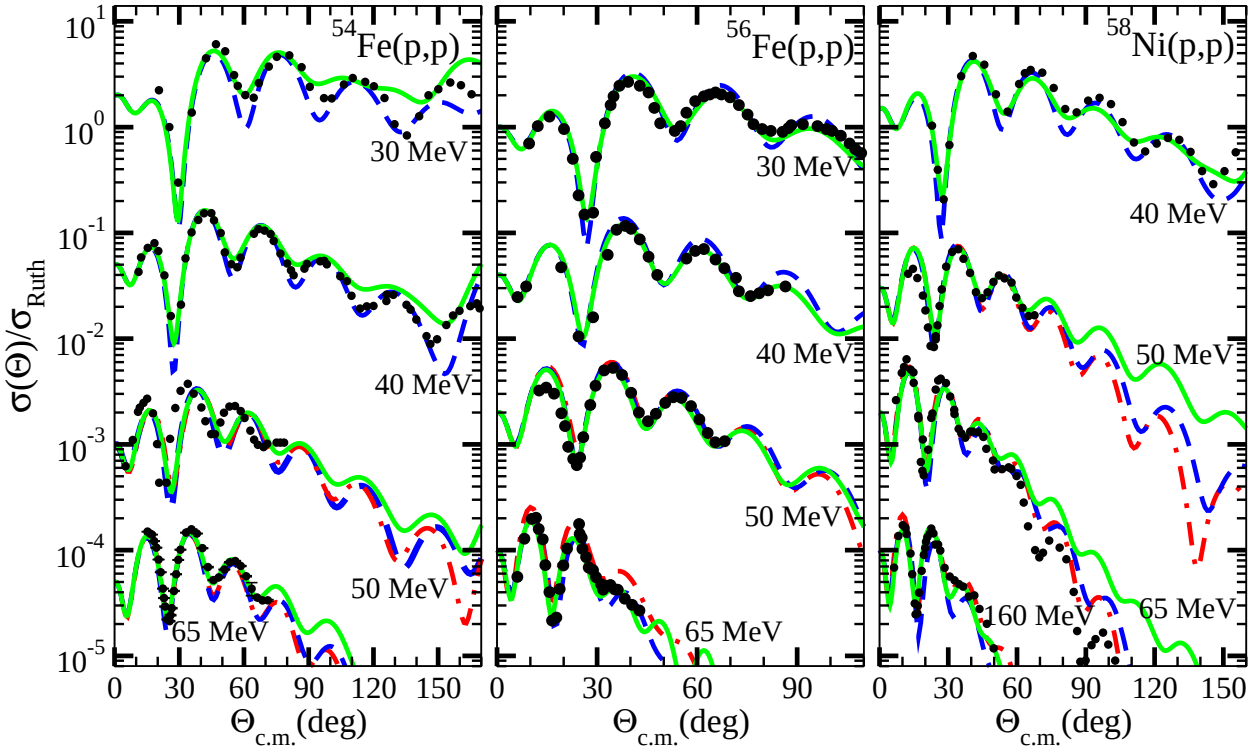

FIG. 8: Proton-nucleus elastic Rutherford reduced differential cross section experimental data for the target nuclei of ^{54}Fe[21, 72, 74, 81], ^{56}Fe[72, 82, 84, 108], ^{58}Ni[84, 109–111], at varying proton laboratory energies. Refer to Fig. 5 for details of the theoretical calculations.

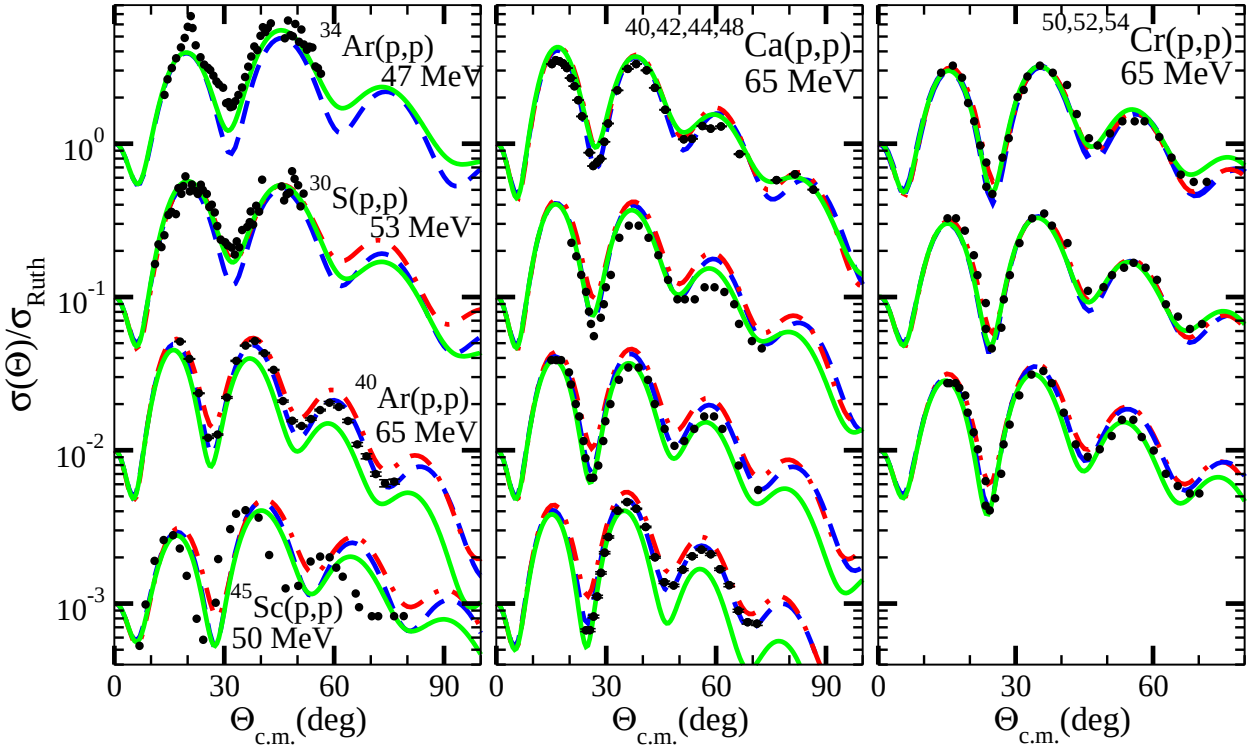

FIG. 9: Proton-nucleus elastic Rutherford reduced differential cross section experimental data for the target nuclei of ^{34}Ar[66, 112], ^{30}S[112], ^{40}Ar[74], ^{45}Sr[72], ^{40,42,44,48}Ca[71, 74], ^{50,52,54}Cr[71], at varying proton laboratory energies. Refer to Fig. 5 for details of the theoretical calculations.

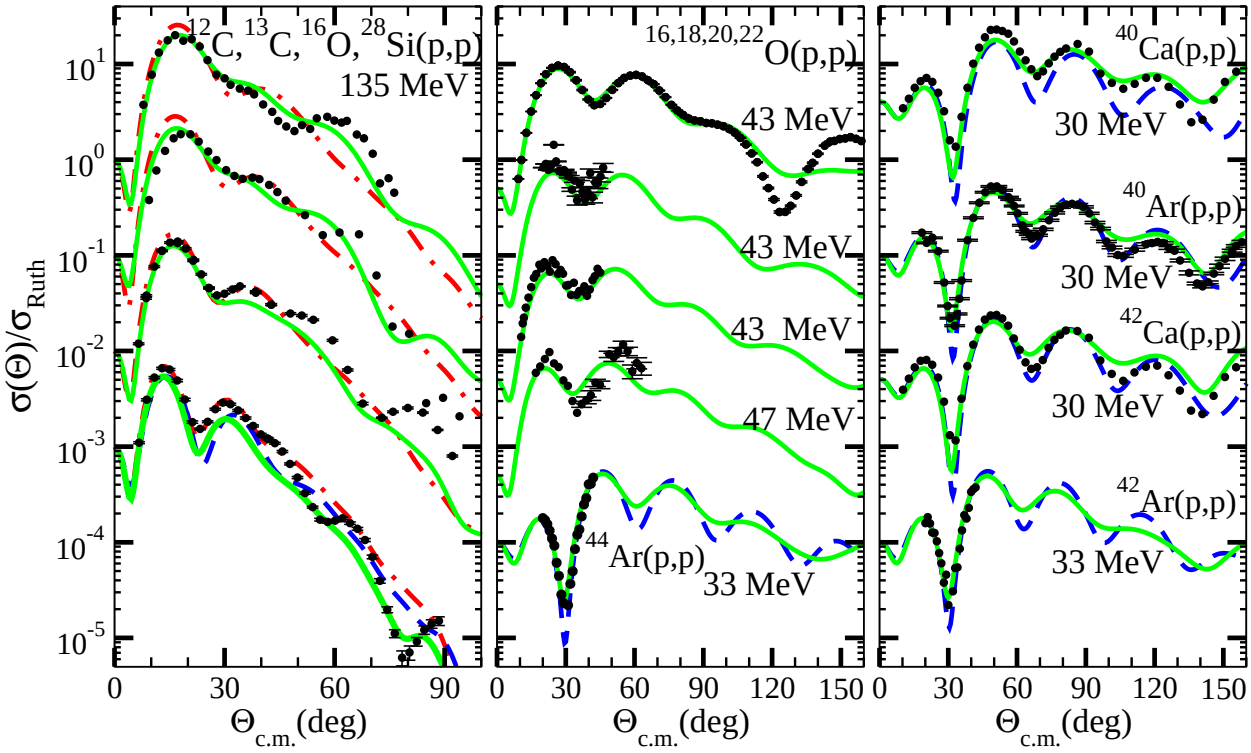

FIG. 10: Proton-nucleus elastic Rutherford reduced differential cross section experimental data for the target nuclei of ^{12,13}C[36, 51], ^{16}O[48, 56], ^{18,20,22}O[50, 57, 112], ^{28}Si[107], ^{40,42}Ca[70, 82], ^{40,42,44}Ar[68, 69], at varying proton laboratory energies. Refer to Fig. 5 for details of the theoretical calculations.

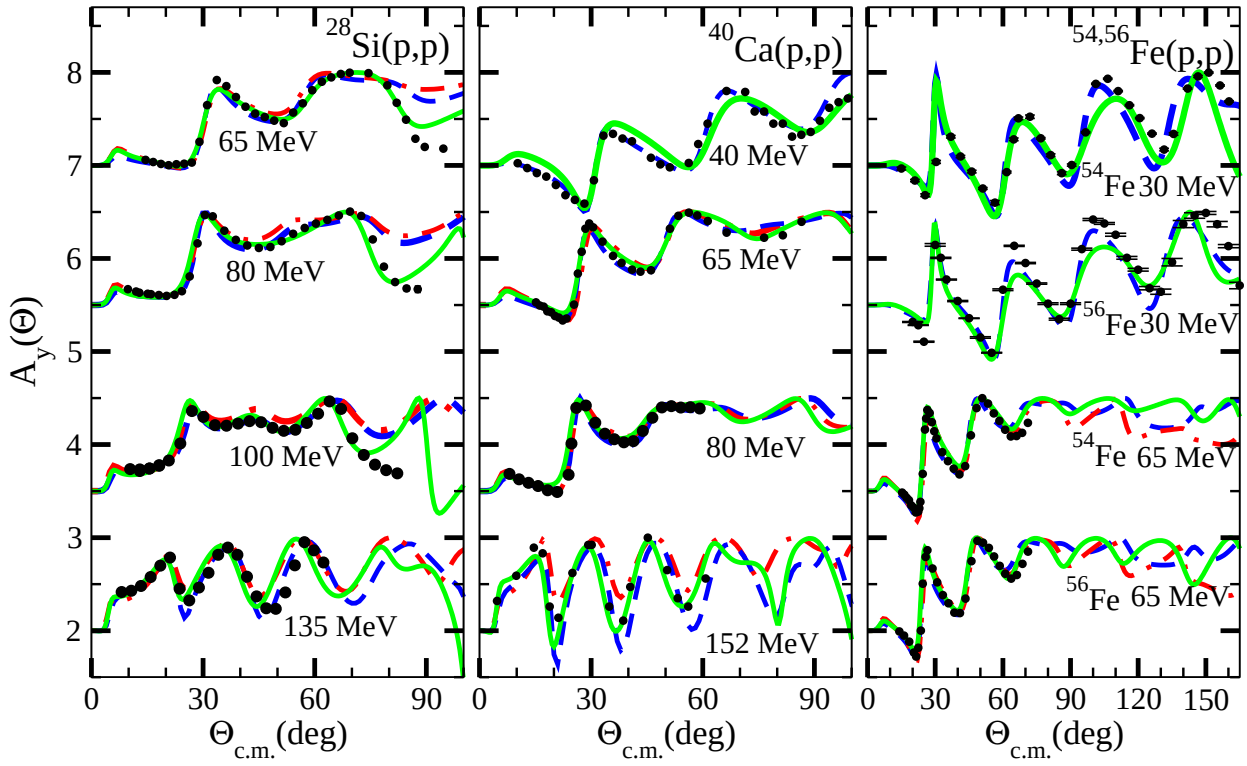

FIG. 11: Proton-nucleus elastic analyzing power spin observable experimental data for the target nuclei of ^{28}Si[74, 107], ^{40}Ca[43, 74, 113, 114], ^{54,56}Fe[21, 74, 84, 115], at varying proton laboratory energies. Refer to Fig. 5 for details of the theoretical calculations.

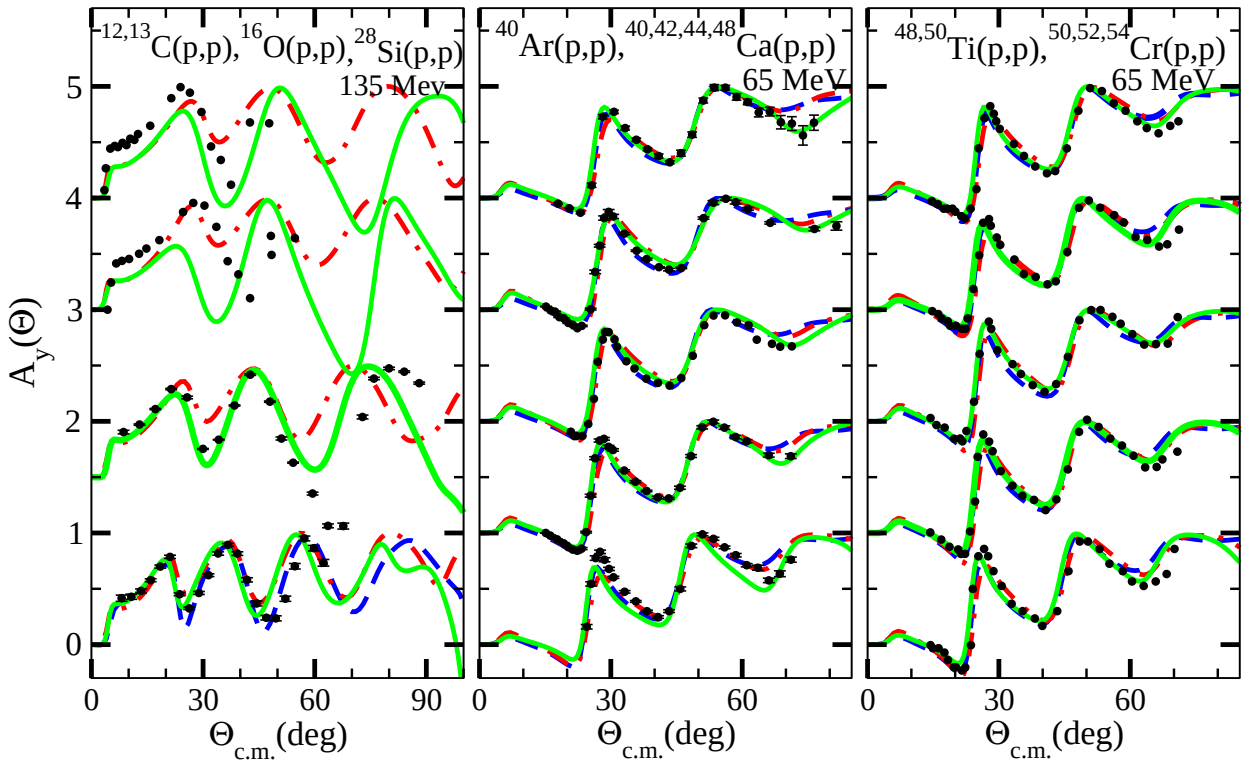

FIG. 12: Proton-nucleus elastic analyzing power spin observable experimental data for the target nuclei of ^{12,13}C[36, 51], ^{16}O[56], ^{28}Si[107], ^{40,42,44,48}Ca[73, 74], ^{40}Ar[52], ^{48,50}Ti[52], ^{50,52,54}Cr[73], at varying proton laboratory energies. Refer to Fig. 5 for details of the theoretical calculations.

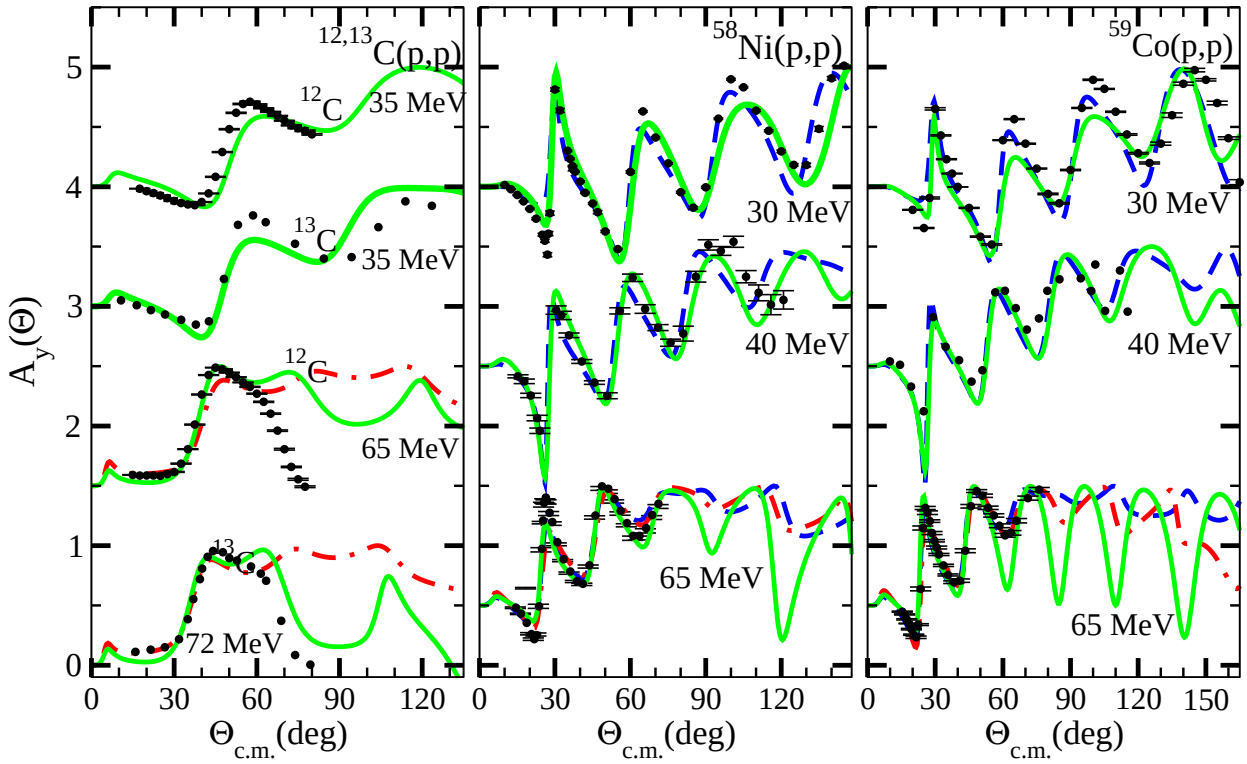

FIG. 13: Proton-nucleus elastic analyzing power spin observable experimental data for the target nuclei of ^{12,13}C[20, 20, 25, 30], ^{58}Ni[84, 109, 116], ^{59}Co[83, 84, 115], at varying proton laboratory energies. Refer to Fig. 5 for details of the theoretical calculations.

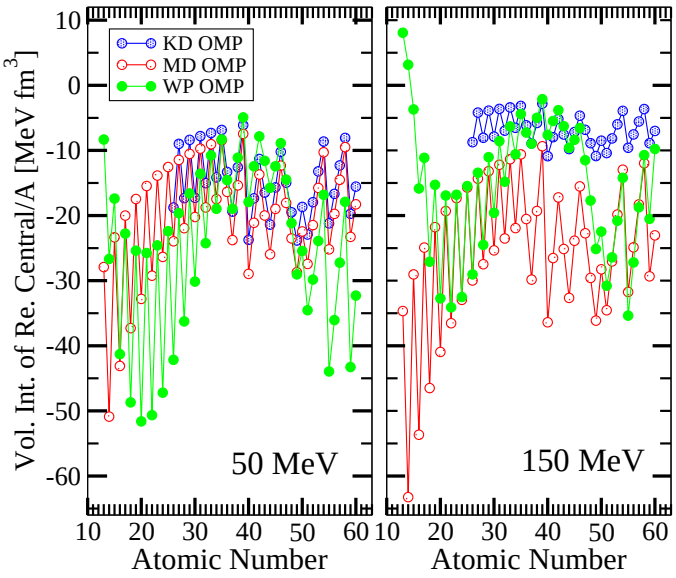

FIG. 14: This is a calculation of the difference in the real component of the central volume integrals between a proton and neutron projectile for a representative selection of nuclei using three different global optical potentials. The nuclei were chosen to have nonzero $N - Z$ terms and to be close or on the line of stability. The nuclei are: ^{13}C, ^{14}C, ^{15}N, ^{16}N, ^{17}O, ^{18}O, ^{19}F, ^{20}F, ^{21}Ne, ^{22}Ne, ^{23}Na, ^{24}Na, ^{25}Mg, ^{26}Mg, ^{27}Al, ^{28}Al, ^{29}Si, ^{30}Si, ^{31}P, ^{32}P, ^{33}S, ^{34}S, ^{35}Cl, ^{36}Cl, ^{37}Cl, ^{38}Ar, ^{39}K, ^{40}Ar, ^{41}K, ^{42}Ca, ^{43}Ca, ^{44}Ca, ^{45}Sc, ^{46}Ti, ^{47}Ti, ^{48}Ti, ^{49}Ti, ^{50}V, ^{51}V, ^{52}Cr, ^{53}Mn, ^{54}Fe, ^{55}Mn, ^{56}Fe, ^{57}Co, ^{58}Ni, ^{59}Co, ^{60}Ni. The blue circular points are the calculation using the KD optical potential [1], the red circular points use the MD optical potential [2] and the filled green circular data points are calculated using the potential of this work. The lines connecting the data points are there to make it easier for the eye to follow. The left panel used a 50 MeV nucleon projectile and the right panel uses a 150 MeV projectile where the differences in the three calculations become more pronounced.

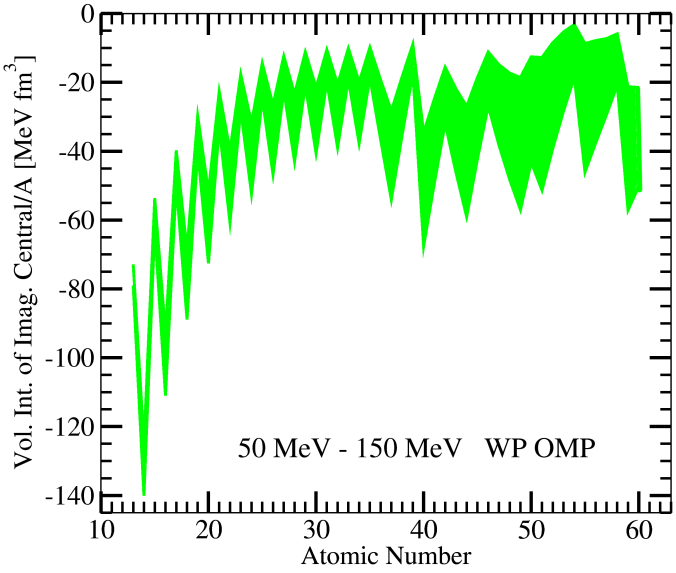

FIG. 15: This is a calculation of the difference in the imaginary component of the central volume integrals between a proton and neutron projectile for a representative selection of nuclei using WP global optical potential. The nuclei were chosen to have nonzero $N-Z$ terms and to be close or on the line of stability. The nuclei are: ^{13}C, ^{14}C, ^{15}N, ^{16}N, ^{17}O, ^{18}O, ^{19}F, ^{20}F, ^{21}Ne, ^{22}Ne, ^{23}Na, ^{24}Na, ^{25}Mg, ^{26}Mg, ^{27}Al, ^{28}Al, ^{29}Si, ^{30}Si, ^{31}P, ^{32}P, ^{33}S, ^{34}S, ^{35}Cl, ^{36}Cl, ^{37}Cl, ^{38}Ar, ^{39}K, ^{40}Ar, ^{41}K, ^{42}Ca, ^{43}Ca, ^{44}Ca, ^{45}Sc, ^{46}Ti, ^{47}Ti, ^{48}Ti, ^{49}Ti, ^{50}V, ^{51}V, ^{52}Cr, ^{53}Mn, ^{54}Fe, ^{55}Mn, ^{56}Fe, ^{57}Co, ^{58}Ni, ^{59}Co, ^{60}Ni. The green fill represents the range possible for nucleon projectile energies between 50 MeV and 150 MeV for the WP global optical potential of this work. The other potentials examined here do not have an isospin asymmetric imaginary component.

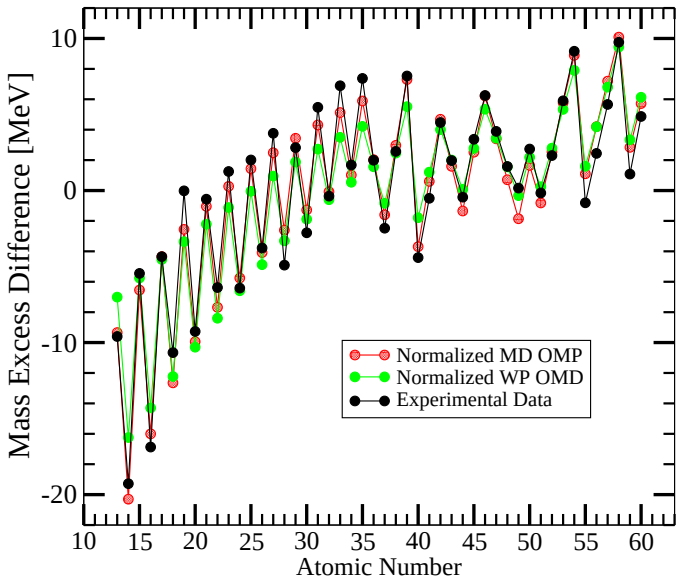

FIG. 16: We plot the total normalized energy difference ($\Delta E_{Re} + \Delta E_{Im}$) for the proton and neutron projectiles on a representative selection of nuclei using two different global optical potentials. The nuclei were chosen to have nonzero $N-Z$ terms and to be close or on the line of stability. The nuclei are: ^{13}C, ^{14}C, ^{15}N, ^{16}N, ^{17}O, ^{18}O, ^{19}F, ^{20}F, ^{21}Ne, ^{22}Ne, ^{23}Na, ^{24}Na, ^{25}Mg, ^{26}Mg, ^{27}Al, ^{28}Al, ^{29}Si, ^{30}Si, ^{31}P, ^{32}P, ^{33}S, ^{34}S, ^{35}Cl, ^{36}Cl, ^{37}Cl, ^{38}Ar, ^{39}K, ^{40}Ar, ^{41}K, ^{42}Ca, ^{43}Ca, ^{44}Ca, ^{45}Sc, ^{46}Ti, ^{47}Ti, ^{48}Ti, ^{49}Ti, ^{50}V, ^{51}V, ^{52}Cr, ^{53}Mn, ^{54}Fe, ^{55}Mn, ^{56}Fe, ^{57}Co, ^{58}Ni, ^{59}Co, ^{60}Ni. We compare these calculations to the difference in experimental mass excess energies for the charge exchange reactions, $Q(n,p) - Q(p,n)$ from the same targets, the data is from Ref. [126]. The MD calculations, the red circles, have been multiplied by .38 fm^{-3}, the WP calculations, the filled green circles, has been multiplied by .15 fm^{-3}. The experimental mass excess energies were not used to constrain the theoretical potentials during the fitting procedure.